Journal Pre-proof

RNA-binding motif 4 promotes angiogenesis in HCC by selectively activating VEGF-A expression

Hexu Han, Ting Lin, Zhenyu Wang, Jingjing Song, Ziyi Fang, Jing Zhang, Xiaomin You, Yanping Du, Jun Ye, Guoxiong Zhou

PII: S1043-6618(22)00539-4

DOI: https://doi.org/10.1016/j.phrs.2022.106593

Reference: YPHRS106593

To appear in: *Pharmacological Research*

Received date: 11 October 2022
Revised date: 23 November 2022
Accepted date: 30 November 2022

Please cite this article as: Hexu Han, Ting Lin, Zhenyu Wang, Jingjing Song, Ziyi Fang, Jing Zhang, Xiaomin You, Yanping Du, Jun Ye and Guoxiong Zhou, RNA-binding motif 4 promotes angiogenesis in HCC by selectively activating VEGF-A expression, *Pharmacological Research,* (2022) doi:https://doi.org/10.1016/j.phrs.2022.106593

RNA-binding motif 4 promotes angiogenesis in HCC by selectively activating VEGF-A expression

Hexu Han[1], Ting Lin[2], Zhenyu Wang[3], Jingjing Song[4], Ziyi Fang[5], Jing Zhang[5], Xiaomin You[5], Yanping Du[1], Jun Ye[6,*], Guoxiong Zhou[5, *]

1. Department of Gastroenterology, The Affiliated Taizhou People's Hospital of Nanjing Medical University, Taizhou, Jiangsu 225300, People's Republic of China.

2. Department of Pathophysiology, School of Medicine, Nantong University, Jiangsu, 226001, China

3. Department of pediatric surgery, Affiliated Hospital of Nantong University, Nantong University, Jiangsu, 226001, China

4. Department of Pediatrics, the Second Affiliated Hospital &Yuying Children's Hospital of Wenzhou Medical University, Wenzhou, 325027, Zhejiang, China

5. Department of Gastroenterology, Affiliated Hospital of Nantong University, Nantong University, Jiangsu, 226001, People's Republic of China

6. Center for Translational Medicine, The Affiliated Taizhou People's Hospital of Nanjing Medical University, Taizhou, Jiangsu 225300, People's Republic of China.

* Correspondence should be addressed to Guoxiong Zhou, Department of Gastroenterology, Affiliated Hospital of Nantong University, 19 Qixiu Road, Nantong, China, 226001, E-mail: zhougx@ntu.edu.cn

Jun Ye, Central laboratory, The Affiliated Taizhou People's Hospital of Nanjing Medical University, Taizhou, Jiangsu 225300, People's Republic of China, Email: m13625171902@163.com

Lists of Abbreviation

Hepatocellular carcinoma (HCC)

Nuclear factor-kappa B (NF-kB)

RNA-binding motif proteins (RBMs)

IGF2 mRNA binding protein 2 (IMP2)

American Type Culture Collection (ATCC)

Human umbilical vascular endothelial cell (HUVEC)

Fetal bovine serum (FBS)

Endothelial Cell Medium (ECM)

Phosphate-buffered saline (PBS)

Hematoxylin and eosin (H&E)

Enzyme-linked Immunosorbent assay (ELISA)

Immunohistochemistry (IHC)

Diaminobenzidine (DAB)

Abstract

Increased angiogenesis in the liver plays a critical role in the progression of hepatocellular carcinoma (HCC). However, the molecular mechanism underlying increased angiogenesis in HCC is not well understood. Current study was designed to identify the potential angiogenic effect of RNA-binding motif 4 (RBM4)through a small-scale overexpression screening, followed by comparison of the expression level of RBM4 in cancer and adjacent tissues in multiple malignancies to explore the relationship between RBM4 and CD31 protein expression level and related clinical indicators, and understand the role of RBM4 in the hepatocellular carcinoma . To understand the specific mechanism of RBM4 in detail, transcriptome sequencing, mass spectrometry and multiple molecular cytological studies were performed. These cellular level results were verified by experiments in animal models of nude mice. The increased expression of RBM4 in cancer tissues, suggested its use as a prognostic biomarker. The RBM4 expression was found to be strongly correlated with tumor microvessel density. Mechanistically, RBM4 mediated its effects via interaction with HNRNP-M through the latter's WDR15 domain, which then stabilized RelA/p65 mRNA. Consequently, RBM4 induced the activation of the NF-kB signaling pathway, upregulating the expression of proangiogenic factor VEGF-A. The results confirmed the mechanism by which RBM4 promotes angiogenesis in hepatocellular carcinoma suggesting RBM4 as a crucial promoter of angiogenesis in HCC, helping understand regulation of NF-kB signaling in HCC.

Keywords: RBM4, metastasis, neovascularization, NF-kappa B, prognosis, p65

Introduction

Hepatocellular carcinoma (HCC) is one of the most common malignancies globally, having a high potential for vascular invasion,and metastasis. The postoperative recurrence is a key reason of poor prognosis for patients suffering from HCC [1]. Angiogenesis, an important characteristic of cancer [2], can be induced early during the development of invasive cancers in both animal models and humans [3]. Angiogenesis is a key aspect of tumor growth and metastasis, besides being a key predictor of overall survival in cancer patients [4], including HCC [5]. Majority of patients do not opt radical treatment because of early intrahepatic vascular metastasis through the portal vein system [6]. However, the molecular mechanism underlying angiogenesis in HCC is unclear.

Nuclear factor-kappa B (NF-kB) is an important transcription factor that helps in the angiogenesis regulation [7]. Excessive and prolonged activation of the classical and non-classical NF-kB signaling pathway has been observed in various human diseases [8] [9]. Hence, aberrant NF-kB activation should be prevented to avoid development and progression of diseases [10]. The dominant cellular form of NF-kB is a heterodimer composed of p50/105 and RelA/p65 subunits, which is normally sequestered in the cytoplasm of non-stimulated cells. The exposure of cells to inflammatory stimuli, leads to the phosphorylation of p65 , and subsequent translocation into the nucleus [11]. In most cases, termination of NF-kB activity requires the proteasomal degradation of nuclear p65 [12]. It is, however, unclear whether there is any other mechanism for terminating the aberrant NF-kB signaling activation, specifically related to the angiogenesis in HCC. RNA-binding motif proteins (RBMs) are a superfamily of proteins having an RNA-binding domain, participating in various post-transcriptional RNA regulation process. For example, RBM3 interacts with IGF2 mRNA binding protein 2 (IMP2) to stimulate the differentiation of corresponding brain regions reducing damage after hypoxic-ischemic brain injury [13]. RBM5, 6, and 10, regulate NUMB alternative

splicing synergistically, influencing the lung cancers [14]. RBM15 is involved in the occurrence and development of many diseases by participating in the RNA methylation [15]. However, its role in HCC neovascularization has not yet been reported. Based on these previous studies, we screened the RNA-binding protein family. It was observed that during RBM4 overexpression in HCC cells, the supernatant can strongly promote the tube formation in human umbilical vein endothelial cells. cells. These findings revealed that RBM4 mediates its effects via interaction with HNRNP-M through the latter's WDR15 domain, thereby stabilizing RelA/p65 mRNA. These findings offer deeper insights into the role of RBM4 in tumorigenesis, illustrating its potential as a new target for anti-angiogenic cancer treatment.

Materials and methods

Cell culture

The human HCC cell lines namely Huh7, HepG2, PLC/PRF/5, Hep3B, SNU-398, SNU-182,and SNU-387 were from American Type Culture Collection (ATCC). The human HCC cell lines MHCC97-H and Lm3;the human embryonic kidney cell line 293T (HEK-293T) and human umbilical vascular endothelial cell (HUVEC) were purchased from Shanghai Institutes for Biological Sciences, Chinese Academy of Sciences. Cell lines including Huh7, HepG2, MHCC97-H, Lm3, and HEK-293T were cultured in DMEM Medium; SNU-398, SNU-182, and SNU-387 were cultured in RPMI-1640 medium; Hep3B was cultured in EMEM medium; and PLC/PRF/5 was cultured in MEM medium. Followed by addition of 10% fetal bovine serum (FBS), penicillin (100 U/mL) , and streptomycin (100 μg/mL), cells were cultured in a humidified chamber with 5% CO_2 at 37 °C. Endothelial Cell Medium (ECM) was used to culture HUVECs . The cells were tested regularly for mycoplasma by R&D Systems' new MycoProbe Mycoplasma Detection Kit And cell lines were validated for short tandem repeat fingerprinting (Shanghai FUHENG Biotechnology Co., Ltd.).

Patients and tissue specimens

The tissue chips (Shanghai Outdo Biotech Co., Ltd. from Shanghai, P. R. China) containing 75 paraffin-embedded HCC samples and corresponding noncancerous tissues from patients diagnosed (histopathologically and clinically) with hepatocellular carcinoma (HCC) were analyzed. Out of these, 28 HCC specimens and matched adjacent noncancerous tissues were from patients who were diagnosed at the Affiliated Hospital of Nantong University. None of the patients received any preoperative cancer treatment. Written informed consent was obtained from all patients. Ethical approval from the Institutional Research Ethics Committee was obtained before the start of the study.

Animal studies

The laboratory animal center of Nantong University provided male BALB/c athymic nude mice (4–6-week-old) . The mice were housed under standard conditions as per the institutional guidelines for animal care. All animal experiments were approved by the Institutional Animal Care and Use Committee of Nantong University. The subcutaneous neoplasia mouse model was designed by by injecting 2×10^6 cells in 100 μl of phosphate-buffered saline (PBS) subcutaneously to the nude mice. Immunohistochemistry (IHC) of excised subcutaneous tumors was performed after 4 weeks. The tail vein metastasis mice model was established by injecting 2×10^6 cells in 100 μl of PBS into the tail vein of nude mice. The lung tissues were excised and subjected to thehematoxylin and eosin (H&E) staining after 4 weeks.

Enzyme-linked Immunosorbent assay (ELISA)

To measure the human VEGF-A levels, different types of cells were placed in 6 cm dishes equally (2×10^6 cells in each dish after counting). After 24 hours, supernatant was collected and centrifuged to remove impurities. Human VEGF-A concentration in supernatant was determined by ELISA by a commercial kit (Quanzhou Ruixin Biological Technology Co., Ltd).

Tube formation assay

A 96-well plate coated with Matrigel (354234, BD Biosciences) was kept at 37°C for 30 min. Before that, HUVEC cells were starved overnight and cultured in different groups of supernatants for 24 hours (the collection method being consistent with the steps in ELISA). HUVECs (2×10^4)were suspended in 100 μl of corresponding groups of supernatants and placed on the pre-coated 96-well plate. After incubation at 37°C for another 6 h, micrographs were taken by a microscope.

***In vivo* Matrigel angiogenesis assay**

Male BALB/c athymic nude mice (4–6 weeks old) were obtained from the laboratory animal center of Nantong University, and were housed under standard conditions according to the institutional guidelines for animal care. All animal experiments were approved by the Institutional Animal Care and Use Committee of Nantong University. A mixture of 500 μl Matrigel (Corning) and corresponding cell supernatant was subcutaneously injected into the dorsal side of mice. Two Matrigel plugs were implanted in each mouse. Matrigel plugs were retrieved from euthanized mice after five days.

Plasmid construction and Lentiviral production

The cDNA of RBM4, HNRNP-M, IKK-β, RelA, and corresponding domains were synthesized and cloned into pcDNA3.1-Hygro-N-3HA, pcDNA3.1-Puro-C-3Flag, pCMV-G418-C-Myc and pGL4.10-hRluc vectors respectively. Guide RNA (gRNA) oligonucleotides were cloned into the lentiCRISPRv2-puro or lentiCRISPRv2-Blast vector to create corresponding plasmids.

The lentivirus was purchased form Genechem (Shanghai, China).

OV-RBM4-F: TCTAGAATGGTGAAGCTGTTCATCGGA

OV-RBM4-R: GGATCCAAAGGCTGAGTACCGCGCC

OV-YY1-F: TCTAGAATGGCCTCGGGCGACACC

OV-YY1-R: GGATCCCTGGTTGTTTTTGGCCTTAGCA

OV-p65-F: GGATCCATGGACGAACTGTTCCCCCT

OV-p65-R: TCTAGAGGAGCTGATCTGACTCAGCA

OV-c-Myc-F: TCTAGACTGGATTTTTTTCGGGTAGTGG

OV-c-Myc-R: GGATCCCGCACAAGAGTTCCGTAGCTG

OV-N-Myc-F: CTAGAATGCCGAGCTGCTCCACG

OV-N-Myc-R: GGATCCGCAAGTCCGAGCGTGTTCA

OV-HES1-F: TCTAGAATGCCAGCTGATATAATGGAGAAAAAT

OV-HES1-R: GGATCCGTTCCGCCACGGCCTCCA

OV-TP63-F: TCTAGAATGAATTTTGAAACTTCACGGTGTG

OV-TP63-R: GGATCCCTCCCCCTCCTCTTTGATGC

OV-IKKB-F: GGATCCATGAGCTGGTCACCTTCCCTG

OV-IKKB-R: TCTAGATGAGGCCTGCTCCAGGCA

OV-HNRNP-M-F: GGATCCATGGCGGCAGGGGTCGAA

OV-HNRNP-M-R: TCTAGAAGCGTTTCTATCAATTCGAACGTC

OV-N-RBM4-F: TCTAGAATGGTGAAGCTGTTCATCGGA

OV-N-RBM4-R: GGATCCTGAACGATCTATCGGACACTCTTT

OV-C-RBM4-F: TCTAGAATGGGCCGCGTGGCAGACTTG

OV-C-RBM4-R: GGATCCAAAGGCTGAGTACCGCGCC

sg-RBM4: GCCCCGGGAGGCTACAGAGC

sg-HNRNP-M: CGGCGACGGAGATCAAAATGG

sg-M-A: CGCTCACACAAAGCCCAGACG

sg-M-B: TAACCATTTTAATTTGTTGGC

sh-p65-1: CGGATTGAGGAGAAACGTAAA

sh-p65-2: CACCATCAACTATGATGAGTT

sh-RBM4-1: CCTGTTCTTCTGTCCTTCAAT

sh-RBM4-2: GCCAAGTTTGAGGAGTATGGT

sh-HNRNP-M-1: CGAATTGATAGAAACGCTTAA

sh-HNRNP-M-2: CTGTGCAAGCTATATCTATGT

RNA extraction, reverse transcription, and real-time RT-PCR

The RNA-easy Isolation Reagent (#C112, Vazyme, Nanjing, China) was used to extract total RNA from cultured cells or fresh tissues. The total RNA was quantified by Nanodrop 1000 spectrophotometer (Thermo Fisher Scientific, USA). Approximately 1 μg RNA was used for the reverse transcription reaction with HiScript III RT SuperMix for qPCR (+gDNA wiper) (#R323, Vazyme, Nanjing, China). Quantitative real-time PCR was performed thrice with AceQ Universal SYBR qPCR Master Mix (#Q511, Vazyme, Nanjing, China) in a StepOnePlus Real-Time PCR System (Applied Biosystems. Foster City, CA). B-actin mRNA was used as an internal control for each sample, and the Ct value for each sample was normalized to B-actin mRNA.

RT-B-actin-F: TCCCTGGAGAAGAGCTACG

RT-B-actin-R: GTAGTTTCGTGGATGCCACA

RT-IL-6-F: TGAAAGCAGCAAAGAGGCACTGG

RT-IL-6-R: CAGGCAAGTCTCCTCATTGAATCC

RT-IL-8-F: CTGTGTGAAGGTGCAGTTTTGCC

RT-IL-8-R: CGCAGTGTGGTCCACTCTCAATC

RT-VEGF-F: CATCACCATGCAGATTATGCG

RT-VEGF-R: CTATCTTTCTTTGGTCTGCATTCAC

RT-RBM4-F: CCTCAACAAAGTTGCATGTG

RT-RBM4-R: AACTCTGTGTTATCAAGGCC

RT-RelA-F: ATGTGGAGATCATTGAGCAGC

RT-RelA-R: CCTGGTCCTGTGTAGCCATT

RT-YY1-F: CCTCTCAGATCCCAAACAACTG

RT-YY1-R: GCCTTTATGAGGGCAAGCTATT

Western blot assays and nuclear and cytoplasmic fraction analysis

All cells and fresh tissues followed by lysis in radioimmunoprecipitation (RIPA) buffer (Beyotime, Shanghai, China) supplemented with 1% proteinase inhibitor (Beyotime, Shanghai, China), were analyzed through a BCA kit (Biosharp, Wuhan, China). An equal

amount of total protein from each sample was separated by 8/10/12% SDS-PAGE and transferred to PVDF membrane.

Preparation of the cytoplasmic and nuclear extracts: cells were lysed on ice for 20 min in hypotonic buffer (10 mM HEPES, pH 7.8, 10 mM KCl, 0.1 mM EDTA, 1 mM PMSF). After centrifugation of samples at 12,000 rpm for 20 min of lysed cells, supernatants were collected for future use as cytoplasmic fractions. The resulting pellets were lysed for 30 min on ice in a hypertonic buffer (20 mM HEPES, pH 7.8, 0.5 M NaCl, 1 mM EDTA, 1 mM PMSF) and vortexed briefly. After another centrifugation for 15 min at 12,000 rpm, supernatants were collected as nuclear fractions.

Immunofluorescence and Immunohistochemistry (IHC)

Cells were cultured on coverslips, rinsed in PBS, fixed for 20 min with 4% formaldehyde, and permeabilized with 0.5% Triton X-100 for 15 min at room temperature. For Immunofluorescence analysis, RBM4 (1:200, proteintech) and HNRNP-M (1:100, Santa Cruz)were used as antibodies. Cell nuclei after stained with Hoechst 33258 (Beyotime, Shanghai, China) were observed under a LEICA TCS SP5 confocal microscope

For immunohistochemistry (IHC) analysis, paraffin-embedded sections were incubated in 3% acetic acid:0.1% trypsin solution at 37°C for 15 min to retrieve the antibodies. Sections were then blocked in normal goat serum (5%, v/v) for 2 h at room temperature. Primary antibodies were diluted in normal goat serum (5%, v/v) and incubated overnight at 4°C in a humidified chamber. Biotin-labeled secondary antibodies were used and visualized by 3,3-Diaminobenzidine (DAB).

Drugs, Antibodies and Reagents

Mouse monoclonal anti-RBM4 (sc-373852), anti-RelA (sc-8008), anti-Myc (sc-40), anti-HA (sc-7392), anti-PCNA (sc-56) , anti-HNRNPM (sc-20002), anti-YY1 (sc-7341), anti-TAK1 (sc-7967), anti-p-STAT3 (sc-8059), anti-p-c-Fos (sc-81485), anti-p-c-Jun (sc-822), anti-VE-cadherin (sc-9989), anti-HIF-1a (sc-13515), anti-VHL (sc-135657) and anti-p53 (sc-126) antibodies and protein A/G PLUS-agarose beads (sc-2003) were

procured from Santa Cruz Biotechnology, with dilution of 1:500. Antibodies namely anti-RBM4 (11614-1-AP), anti-Flag (20543-1-AP), anti-myc-tag (16286-1-AP), anti-IKKB (15649-1-AP), anti-p50/105 (14220-1-AP), anti-Fos (66590-1-Ig), anti-JUN (66590-1-Ig) and anti-GAPDH (66590-1-Ig,1:10000) were obtained from ProteinTech (Wuhan, China). Polyclonal rabbit antibodies anti-IKK alpha (GB11923) and anti-Ki67 (GB14102) were obtained from Servicebio (Wuhan, China). Anti-STAT3 (#12640), anti-IKba (#4814), anti- Phospho-IKKα/β (Ser176/180) (#2697), anti-phospho IKba (Ser32/36) (#9426), anti-NF-κB p65 (Ser536) (#3033) and SimpleChIP® Plus Enzymatic Chromatin IP Kit (Magnetic Beads) #9005 were procured from Cell Signaling Technology. Anti-CD31 (ab9498) was purchased from Abcam. Mouse monoclonal anti-FLAG (F1804) antibody and formaldehyde were purchased from Sigma-Aldrich (St. Louis, MO, USA). Actinomycin D was from BioVision, Bay11-7082 and IMD-0354 were purchased from Medchem Express (Monmouth Junction, New Jersey, USA). Recombinant human TNF-α was obtained from PeproTech. Cell Counting Kit-8 was obtained from Vazyme (#A311, Vazyme, Nanjing, China). The remaining antibodies were diluted as 1:1000.

Dual-luciferase reporter gene assays

Using pGL4.10-hRluc reporter vector (which carries two proteins of sea kidney fluorescence and firefly fluorescence), KpnI (NEB, R3142) was first used for enzyme digestion and gelling recovery, then BglII (NEB, R0144) was used for enzyme digestion and gelling recovery. Synthetic containing p65 combination of classic sequence "GGGAATTTCCGGGAATTTCCGGGAATTTCCGGGAATTTCC" insert fragment, after annealing, T4 ligase is inserted to pGL4.10 - hRluc report gene carrier, the conversion coating after the board and pick monoclonal amplification sequencing verify correct, For subsequent cell experiments. The above construct successful pGL4.10-hRluc-NF-kB reporter plasmid respectively into the above construction of different stable transfer cell lines, using multifunctional microplate detector (BiotekHTX)

according to the Dual Luciferase Reporter Assay Kit (vazyme, DL101) instructions, with kidney fluorescence as a reference, compare the relative intensity of firefly fluorescence, so as to determine the cell of NF-kB signaling pathway activity.

Bioinformatics Analysis

Datasets: The transcriptome RNA-seq profiles and corresponding clinical information of TCGA-SKCM samples were downloaded from Genomic Data Commons (https://portal.gdc.cancer.gov/). The expression profiles were transformed into transcripts per million (TPM) for downstream analysis. RNA-seq and sample profiles (GSE76427) used for validating the accuracy of RBM4 expression were obtained from the Gene Expression Omnibus (GEO) database. The probe ILMN_1709042 was used for matching the RBM4.

Survival analysis: The TCGA-Clinical Data Resource (CDR) was used to obtain overall survival (OS), disease-specific survival (DSS), disease-free survival (DFS) and progression free survival (PFS) results of the liver hepatocellular carcinoma (LIHC) samples. . The “survival” package was used to construct Kaplan–Meier curves with the log-rank test. The “maxstat” R package determined the best cutoff and divided it into RBM4-low or RBM4-high groups. The clinicopathological factors, and the RBM4 expression, were used for univariate and multivariate Cox regressions analysis by the “survival” package. Only significant factors with a p-value < 0.05 in the univariate analyses were used in multivariable analyses. Cox regression results were in two significant digits.

Statistical Analysis: The Mann–Whitney test or Wilcoxon signed-rank test for two-group analysis was used. Kruskal–Wallis one-way analysis of variance (ANOVA) was used for comparisons between the different groups. Bonferroni's multiple comparisons test was used for pairwise comparison between multiple groups. Survival analysis and gene expression analysis were conducted in R version 4.0.0 and Graphpad Prism 8.1.0.

Co-Immunoprecipitation（Co-IP）and Mass spectrometry (MS) analysis

For immunoprecipitation, cells were washed with ice-cold phosphate-buffered saline (PBS) on ice. Whole cell lysates were prepared in IP buffer (20mM Tris(pH7.5), 150mM NaCl, 1% Triton X-100 ， 0.1 mM sodium pyrophosphate, 25 Mm β-glycerophosphate, 3 mM EDTA and 1 mM PMSF) and mixed with protein A/G PLUS-agarose beads. The resulting mixture was rotated for 2 h at 4°C, followed by centrifugation at 12000 rpm for 5 min, and the supernatant obtained was used for immunoprecipitation. The protein A/G PLUS-agarose beads were coated with corresponding antibody for 2 h at 4°C, and washed extensively by IP buffer containing PMSF. The precleared lysate was diluted with IP buffer, mixed with the antibody-coated beads and incubated with rotation overnight. The pre-cold washing buffer (20 mM HEPES, pH 7.7, 50 mM NaCl, 2.5 mM MgCl2, 0.1 mM EDTA, 0.05% Triton X-100 and 1 mM PMSF) was used to wash precipitates thrice .The beads were resuspended in 2X sample buffer and boiled for 10 min. Immunocomplexes were analyzed by SDS-PAGE and immunoblotting was analyzed by mass spectrometry (MS) (Shanghai Biotree Biomedical Technology Co, Ltd, China)

RNA immunoprecipitation (RIP)

Cells collected were washed twice with ice-cold PBS, and resuspended in PBS (2 ml). Formaldehyde (37% stock) was added to the solution to a final concentration of 1% followed by incubation for 20 min at room temperature. Glycine solution (pH 7.0) was added to a final concentration of 0.2 M followed by a 10 min incubation at room temperature to terminate the crosslinking reactions . Cells were collected by centrifugation at 1000 rpm for 3 min at 4°C, followed by 2 washes with ice-cold PBS. Fixed cells were resuspended in 1 ml of radioimmunoprecipitation assay (RIPA) buffer (50mM Tris (pH 7.4), 150mM NaCl, 1% NP-40, 0.5% sodium deoxycholate，0.1% SDS and 1mM PMSF). The samples were sonicated at 30% amplitude for three cycles of 30s (3s on, 3s off) with a 1-min gap between cycles and mixed with protein A/G

PLUS-agarose beads. This mixture was rotated for 2 h at 4°C and centrifuged at 12,000 rpm for 5 min. The supernatant was removed and used for immunoprecipitation. Protein A/G PLUS-agarose beads were coated with the corresponding antibody for 2 h at 4°C, and thoroughly washed with RIPA buffer containing protease inhibitors. The RIPA buffer was use to dilute the precleared lysate , mixed with the antibody-coated beads, and incubated with rotation overnight. A minicentrifuge (@1,000 rpm for 3 min) followed by 5 washes with RIPA buffer (1 ml) was used to collect the beads. Beads containing the immunoprecipitated samples were collected and resuspended in 100 µl of buffer (50 mM Tris-Cl, pH 7.0, 5 mM EDTA, 10 mM dithiothreitol and 1% SDS). Samples (resuspended beads) were incubated at 70°C for 45 min to reverse the crosslinks. RNA was extracted from these samples using RNA-easy isolation reagent and reverse-transcribed into cDNA for PCR detection.

RIP-RelA-F: ATGTGGAGATCATTGAGCAGC

RIP-RelA-R: CCTGGTCCTGTGTAGCCATT

Chromatin immunoprecipitation (ChIP)

Cells were treated with 1% formaldehyde for 10 min in a 100mm culture dish to crosslink chromatin-associated proteins to DNA. Glycine was added to quench the unreached formaldehyde. Cells were collected in 1 ml lysis buffer and sonicated at 40% output to shear the DNA to 200–1000-bp fragments. The lysates were cleared by centrifugation at 12,000 rpm for 10 min at 4 °C. Lysates (100 µl) were mixed with dilution buffer (900 µl), followed by addition of protein A/G PLUS-agarose beads and incubating for 2 h at 4 °C to preclear the chromatin. The precleared lysates were incubated with the corresponding antibody overnight at 4 °C with rotation. The RT-PCR was done affter protein/DNA complexes were reverse cross-linked to free DNA.

ChIP-RBM4-F: AGTTGGCGCCATGAAGCTAA

ChIP-RBM4-R: AGAGAACGGGTTAGTCGCTC

Purification of recombinant proteins

The GST-tagged constructs in pGEX-6P-1 vector and His-tag constructs in pET-28a vector were transformed into *E. coli* strain BL21 (DE3) and incubated with 0.2 mM IPTG (Biosharp, BL545A) at 25 ℃ overnight for induction of expression of recombination proteins . GST-tag and His-tag proteins were purified using Glutathione Sepharose 4B beads (GE Healthcare, #17075601) and HISTRAP FF (GE Healthcare, #11000458) respectively, following the manufacturer's instructions. The purified proteins were instantly used for the experiments or frozen at −80 ℃.

Statistical analysis

All cytology assays (including CCK8 assays, wound healing assays, tube formation assays, qPCR assays, and ELISA assays) were performed in three independent replicates. For animal experiments in *in vivo* Matrigel angiogenesis assays, were performed in four independent replicates, and in tail vein metastasis mice model and subcutaneous tumorigenesis in nude mice model, were performed in five independent replicates. The GraphPad Prism7 software was used to assess the statistical significance of differences between groups while significance between groups was measured by Student's t-test or one-way ANOVA . Statistical analyses between different treatments, in different cell cohorts or at different time points were performed using two-way ANOVA. The overall survival was assessed according to the Kaplan-Meier method and significance was evaluated by the log-rank test. The intensity of RBM4 staining between the CD31 and p-p65 was quantified by Image-Pro Plus6 and their correlations was analyzed by Chi-square test (Fisher's exact). Statistical significance was concluded at *$P < 0.05$, **$P < 0.01$, ***$P < 0.001$; ns represents no statistical significance.

Results

Role of RBM4 in tumor angiogenesis promotion

To explore the role of RBP superfamily in the promotion of HCC angiogenesis, a library of mammalian expression vectors encoding 20 RBPs was generated and separately transfected into Huh-7 cells (Fig. 1A). Tube formation assays were used to evaluate the angiogenesis-stimulating effects of supernatant from different Huh7-ov-RBP cells. This experiment indicated that the supernatant from Huh-7-ov-RBM4 cells significantly promoted the formation of complete tubular structures, while the supernatant from Huh7 cells overexpressing other RBPs had marginal or no effects (Fig. S1A). The RBM4 expression levels in different HCC cell lines were examined (Fig. S1B), to evaluate gain- or loss-of-functions in differently transfected cells. Multiple HCC cell lines were used to confirm the above findings. The average rate at which complete tubular structures were formed by HUVECs was substantially higher in cells receiving conditioned medium from Huh-7/PLC/PRF-5-ov-RBM4 cells and lower in those incubated with medium from HepG2/Hep3B-1-sh-RBM4 cells than the corresponding control cells (Fig. 1B and Fig. S1C,D). To discern the functional role of RBM4 in angiogenesis,we analyzed the *in vitro* HUVEC growth and migration =. The HUVECs growth in conditioned medium from Huh-7/PLC/PRF-5-ov-RBM4 cells was faster than the controls. In contrast, the growth-enhancing effect on HUVECs in conditioned medium from HepG2/Hep3B-1-sh-RBM4 cells were not observed (Fig. 1C). Similar results were observed in the wound healing assay, and confirmed by the statistical results implying that supernatant from cancer cells overexpressing or deficient of RBM4 had opposite effect on the *in vitro* migration of HUVECs (Fig. 1D and Fig. S1E). All this suggested that RBM4 could indeed promote tumor angiogenesis.

Correlation between RBM4 upregulation and increased invasiveness and poor prognosis

To confirm the role of RBM4 in the development of HCC, its expression in HCC tumor tissues and matched paracancerous tissues was measured by Western blotting, which indicated significantly higher RBM4 expression in tumor tissues (Fig. 2A). Supporting Figure S2A illustrates the significant different expression between the two groups. Similar results were observed by qPCR assays in another group of fresh tissues. (Fig. S2A), suggesting key role of RBM4 in tumor development. To verify this conjecture, the RBM4 expression in publicly available datasets was examined. Analysis of TCGA and GEO database showed that RBM4 overexpression in hepatocellular carcinoma tissues (Fig. S2B) and Kaplan–Meier survival analysis revealed that this overexpression is significantly correlated with poor survival (Fig. 2B). RBM4 is also significantly correlated with various clinical parameters (Fig. S2B). Hence, RBM4 expression is upregulated in HCC and could serve as an independent prognostic marker. The analysis of RBM4 expression and microvessel density (MVD) (indicated by CD31-positive cells) in tumor specimens from tissue microarrays containing 75 paraffin-embedded HCC samples and corresponding noncancerous tissues, by using IHC staining revealed high correlation between the two. The increased expression of RBM4 in HCC tissues, increases the MVD during IHC staining -(Fig. 2C, Fig. S2C). These results suggests that RBM4 may affect the prognosis of patients with HCC by promoting tumor neovascularization which was confirmed by various *in vivo* experiments. A mixture of cell supernatants from Huh-7-ov-RBM4/HepG2-sh-RBM4 cells and corresponding controls with Matrigel was injected subcutaneously to mice. Five days later, Matrigel plugs were retrieved and blood vessel formation and perfusion within the Matrigel plugs were evaluated by hematoxylin-eosin staining and immunohistochemistry. Consistent with *in vitro* results, more blood vessels were observed in Matrigel plugs mixed with conditioned medium from Huh7-ov-RBM4 than the control plugs (Fig. 2D and Fig. S2D).However, almost no infiltration of blood vessels in the Matrigel plugs mixed with conditioned medium from HepG2-sh-RBM4 cells was observed compared with the

control plugs (Fig. S2E). In the tail vein metastasis mice model, mice injected with the Huh-7-ov-RBM4 cells had more and bigger lung metastases than the corresponding negative control groups. Mice injected with the HepG2-sh-RBM4 cells had fewer and smaller lung metastases as compared to the corresponding negative control group, as confirmed after histological analysis of the lung tissues from each group (Figure 2E and Fig. S2F).

RBM4 promotes angiogenesis through VEGF-A

The above results suggest that RBM4 can promote the formation of new blood vessels in hepatocellular carcinoma. To explore the specific molecular mechanism, the supernatant of Huh-7/PLC/PRF-5-ov-RBM4 cells and corresponding control cells was collected through Human Angiogenesis Array Kit. The results indicated significantly increased content of VEGF-A in the supernatant from the group of RBM4-overexpressed cells (Fig. 3A) as compared to the control group. The VEGF-A mRNA and protein levels were evaluated by real-time PCR and ELISA, respectively, in different cell lines to confirm this finding. Results revealed that RBM4 can promote the expression and secretion of VEGF-A (Fig. 3B,C). The VEGF-A blocking assays performed to confirm the role of VEGF-A in RBM4 regulated HCC cell angiogenesis, suggested that the VEGF-A antibody repealed the increased tube formation in RBM4 overexpressed cells (Fig. 3D). The corresponding RNA immunoprecipitation results showed that RBM4 does not directly bind to the mRNA of VEGF-A (Fig. S3A).Transcriptomic sequencing using the stable cell lines constructed above indicated that RBM4 can affect angiogenesis in tumors through VEGF-A signaling pathway (Fig. S3B).These findings confirm that RBM4 promotes tumor angiogenesis by increasing the expression and secretion of VEGF-A, thereby influencing the prognosis of patients with HCC.

RBM4 promotes NF-kB activity and the expression of its target pro-angiogenesis genes

Some key molecules of the related signaling pathways enhancing tumor angiogenesis were examined to further explore the specific mechanism by which RBM4 increases the expression of VEGF-A to promote angiogenesis. Especially HIF-1a was studied, as previous reports indicated that RBM4 may have an impact on the expression of HIF-1a in lung cancer cells [16]. Our results revealed that RBM4 had no effect on the expression of HIF-1a or other important molecules in the analyzed targets (Supporting Fig. S4A). Dual-luciferase reporter gene assays was used to investigate role of whether RBM4 in angiogenesis through activation of the NF-kB pathway. Increased luciferase activity was observed in RBM4-overexpression cells compared to the control cells. Contrarily, NF-kB activity was reduced in RBM4-deficient cells, and this reduction was more obvious when exposed to a pathway activator [tumor necrosis factor-a (TNF-a)] in HEK-293T. Subsequently, these RBM4-deficient cells were transfected with different plasmids in the NF-kB pathway to detect the activity at which level the signaling was blocked. The results revealed that signaling became stagnant at the RelA/p65 level (Fig. 4A and Supporting Fig. S4B). Hence, it is suggested that RBM4 might regulate the NF-kB pathway by altering RelA/p65 expression in cells. This hypothesis was validated through qRT-PCR and Western blot assays confirming that the mRNA and protein levels of RelA/p65 were lower when RBM4 was knocked down in different HCC cell lines and knocked out in HEK-293T cells (Fig. 4C and Supporting Fig. S4C). It indicates that RBM4 affects the activity of the NF-kB signaling pathway by regulating RelA/p65 expression. These results also confirmed that no significant change took place in the expression of other proteins of this pathway (Fig. 4D and Supporting Fig. S4D). Immunofluorescence was used to assess the effects of RBM4 on RelA/p65 expression (Supporting Fig. S4E). As RelA/p65 must be translocated into the nucleus to perform its function, protein subfraction analysis suggested that the nuclear translocation of

RelA/p65 was increased by RBM4 overexpression and repressed in different RBM4-deficient cells (Fig. 4E and Supplementary Fig. 4F). Real-time PCR results demonstrated that the increased VEGF-A levels following RBM4 overexpression can be stopped by knocking down RelA/p65 expression by siRNA or suppressing NF-kB activity with a specific inhibitor (Bay-11) (Fig. 4F and Supplementary Fig. 4G). Concludingly, our findings demonstrated that RBM4 regulates the NF-kB signaling pathway by modulating RelA/p65 expression, subsequently affecting VEGF-A expression.

RBM4 recruits HNRNP-M to active NF-kB pathway

The RBM4 stimulating mechanism for the NF-kB pathway was explored by integrating co-immunoprecipitation (Co-IP) with mass spectrometry to identify RBM4 interaction partners (Supporting Fig. S5A). The top 20 possible interacting molecules in the above results with the highest readings were selected and CRISPR/Cas9 was used to screen them in Huh7-ov-RBM4 cells. Preliminary screening suggested that upon knocking out HNRNPM, the increased RelA/p65 expression and p-p65 content caused by the overexpression of RBM4 can be recouped in Huh-7 cells (Supporting Fig. S5B) suggesting HNRNP-M as a potential RBM4 interaction partner. Simultaneously, it was observed that directly knocking out HNRNP-M in HEK-293T and Huh-7 cells alone does not change the content of RelA/p65 and p-p65 and the expression of VEGF-A (Supporting Fig. S5C). The DDX5 can interact with RBM4, selectively attenuating the serine 311phosphorylation of NF-KB p65 subunit in the HEK-293T cells. To determine whether DDX5 is involved in RBM4-mediated angiogenesis in hepatocellular carcinoma, knocking out of DDX5 in Huh7/PLC/PRF/5-ov-RBM4 cells showed that the tube formation of human umbilical vein endothelial cells does not change significantly (Supporting Fig. S5D). The HNRNP-M was designated as the RBM4-mediated interaction protein for angiogenesis in hepatocellular carcinoma. The Co-IP suggested

that the endogenous RBM4-HNRNP-M interaction was confirmed in HEK-293T cells (Fig. 5A) and in two HCC cell lines (HepG2 and Hep3B) (Supporting Fig. S5E), indicating that this interaction could be universal rather than cell line-specific. Since, both RBM4 and HNRNP-M are RBP, the HEK-293T cell lysate was also pretreated with RNase before immunoprecipitation. Results revealed that RNA does not mediate the RBM4–HNRNP-M interaction (Supporting Fig. S5F). This was also confirmed by immunofluorescence assay, suggesting that nucleus is interaction place of RBM4–HNRNP-M (Fig. 5A). The interaction is direct since glutathione S-transferase (GST) or histidine (His) pull-down showed that purified His-tagged HNRNPM protein interacted with purified GST-RBM4, and not GST alone (Fig. 5B). Western blots showed that HNRNP-M knockout in HEK293T or knockdown in Huh-7/PLC/PRF/5 cells compromised the increase in RelA/p65 expression and p-p65 content caused by RBM4 overexpression (Fig. 5C and Supporting Fig. S5G). The dual-luciferase reporter gene assays in Huh7/PLC/PRF/5 cells showed that knocking down HNRNP-M reduces the activity of the NF-KB signaling pathway increased by the RBM4 overexpression (Fig.5D). These results show that the activation of RBM4 in the NF-KB signaling pathway depends on its interaction with HNRNP-M.

Collectively, RBM4 affects the expression of VEGF-A through the NF-KB signaling pathway. The qPCR assay was used to detect whether knocking down HNRNP-M could rescue the VEGF-A mRNA surge caused by RBM4 overexpression in Huh-7/PLC/PRF/5 cells (Supporting Fig. S5H). ELISA was also used to confirm that blocking NF-kB signaling or interfering with HNRNP-M can save the increase in VEGF-A secretion caused by RBM4 overexpression in Huh-7/PLC/PRF/5 cells (Fig. 5E). Tube formation assays suggested that blocking the NF-kB signaling pathway or interference with HNRNP-M can rescue the increased average rate of complete tubular structures stimulated by supernatant from Huh-7-ov-RBM4 or PLC/PRF/5-ov-RBM4 cells (Fig. 5F and Supporting Fig. S5I). The results (Supporting Figure S5J) prove these findings

indicating that the RBM4-mediated upregulation of NF-kB signaling depends on its interaction with HNRNP-M.

The WDR15 domain of HNRNP-M is indispensable for RBM4–HNRNP-M interaction

To map the specific RBM4-interacting region in HNRNP-M, several expression plasmids were constructed with myc-tagged truncated HNRNP-M (M-JD1, M-JD2, M-JD3) and transfected into HEK-293T cells along with the RBM4-FLAG expression plasmid. These Co-IP results revealed that the region spanning residues 301–623 aa of HNRNP-M (WDR15 domain) was needed for its interaction with RBM4 (Fig. 6A). Similarly, constructed FLAG-tagged truncated forms of RBM4 (N-RBM4-Flag, C-RBM4-Flag) were co-expressed with HNRNP-M-myc in HEK-293T cells, followed by Co-IP. The results suggested that the N-terminal of RBM4 (1–200 aa) was involved in the interaction with HNRNP-M (Fig. 6B). Based on above observations, it can be concluded that interaction between RBM4 and HNRNP-M was mediated via the N-terminal of RBM4 and the WDR15 domain of HNRNP-M. *In vitro* protein purification and binding experiments further proved this finding (Supporting Fig. S6A). It was observed that directly knocking out of HNRNP-M did not affect the expression of RelA/p65, while knocking out HNRNP-M could rescue the increase in RelA/p65, consistent with the results obtained in HEK-293T cells. To completely knock out the HNRNP-M gene, two CRISPR-Cas9 plasmids with different targets were used(Supporting Fig. S6B) followed by overexpression of myc-M-JD1, myc-M-JD2 and myc-M-JD3, in Huh7-ov-RBM4-sg-M(A+B) and PLC/PRF/5-ov-RBM4-sg-M(A+B) cells. Compared to the corresponding control cells, only myc-M-JD1and myc-M-JD3 rescued the decline in NF-kB activation in ov-RBM4-sg-M(A+B) cells, It indicates the importance of HNRNP-M, especially its WDR15 domain, in the activation of NF-kB signaling through RBM4 overexpression (Fig. 6C and Supporting Fig. S6C).

ELISA was used to confirm the role of the WDR15 domain in the promotion of VEGF-A expression through RBM4 overexpression (Fig. 6D and Supporting Fig. S6D). These results along with those of the tube formation assays and the corresponding statistical analysis, confirmed the essential role of the WDR15 domain in the promotion of tumor angiogenesis by RBM4 overexpression (Fig. 6E and Supporting Fig. S6E,F).

Requirement of The N-terminal of RBM4 for p65 stability

Although RBM4 enhances the NF-kB signaling activity by interacting with the RBM4–HNRNP-M interaction, the mechanistic significance of the interaction remains unclear. Since RBM4 and HNRNP-M are both RBP, it is necessary to establish whether these can directly bind to RelA/p65 mRNA. To test this hypothesis, we used RNA immunoprecipitation (RIP) assay to spot the potential direct interaction between RBM4 and RelA/p65 mRNA in Huh-7 and PLC/PRF/5 cells (Fig. 7A). Although the HNRNP-M protein did not form a heterodimer with RelA/p65 mRNA in Huh-7 or PLC/PRF/5 cells (Supporting Fig. S7A), RBM4 forms a heterodimer with RelA/p65 mRNA through its N-terminal domain (Fig. 7A) as confirmed in HEK-293T cells (Supporting Fig. S7B). It can be concluded that RBM4 directly binds to RelA/p65 mRNA via its N-terminal domain and uses this domain to recruit HNRNP-M for direct association with the latter's WDR15 domain to form a heterotrimer. RBM4, influences RelA/p65 expression both at the mRNA and protein level. To distinguish between transcriptional and post-transcriptional regulation, transcription was specifically blocked with actinomycin D (ActD). A strong impact of RBM4 on RelA/p65 mRNA stability in multiple cell lines was observed, implying that RBM4 controls the RelA/p65 expression at the post-transcriptional level. Overexpression of RBM4 could stabilize RelA/p65 mRNA, whereas HNRNP-M knockdown partially rescued this phenomenon (Fig. 7B and Supporting Fig. S7C,D) suggesting that RBM4 activates NF-kB signaling by recruiting HNRNP-M to stabilize the RelA/p65 mRNA. Although HNRNP-M does not have a

direct role in this process, it is necessary for this phenomenon. The upstream driving factors influencing the difference of RBM4 expression between the HCC cell lines were explored further. Analysis of the promoter region of RBM4 through University of California Santa Cruz (UCSC), suggested that HES1, c-MYC, YY1, TP63, and other proteins may affect its expression. Relevant overexpression plasmids were constructed and transfected into HEK-293T cells. Only YY1 increased the RBM4 expression (Supporting Fig. S7E). Examination of this YY1 content in different cancer cells suggested a high correlation between YY1 and RBM4 expression (Supporting Fig. S1B). Overexpression or knockout of YY1 in hepatocellular carcinoma cells can affect the expression of RBM4 in the cell (Supporting Fig. S7F). The qRT-PCR and Western blot confirmed that overexpression or knockdown of YY1 in HEK-293T cells affects RBM4 levels similarly (Supporting Fig. 7G). To confirm that YY1 binds directly with the RBM4 promoter, a ChIP assay using chromatin from Huh-7 and PLC/PRF/5 cells was performed. Results revealed that YY1 could directly bind to the RBM4promoter region (Fig. 7C), which was confirmed by dual-luciferase reporter gene assays (Fig. 7D). Literature suggests that YY1 can directly enhance the activity of the NF-kB signaling pathway, enhancing tumor development [17]. Hence dual-luciferase reporter gene and Western blot were used to check this finding. It was observed that RBM4 knockdown can completely block this effect in different cells (Fig. 7E and Supporting Fig. 7H). These findings established that blocking RBM4 can directly inhibit tumor progression besides inhibiting other cancer-promoting signaling pathways, reflecting its clinical potential as a therapeutic target.

In vivo RBM4 overexpression in cancer cells promotes angiogenesis

The paraffin sections suggested higher RBM4 levels in HCC tissue than the corresponding paracancerous sections, and higher RBM4 content was usually accompanied by higher tumor MVD. Higher p-p65 expression was observed in the

RBM4-high group, validating our findings described above, namely a clinically significant correlation between RBM4 and NF-kB activation (Fig. 8A and Supporting Fig. 8A). To explore the RBM4 role in tumorigenesis *in vivo*, stable Huh-7-ov-RBM4 or corresponding vector control cells were injected subcutaneously into nude mice. Accelerated tumor growth was noticed in the RBM4 overexpression group. Interference from HNRNP-M expression potentially delayed this process (Fig. 8B,C and Supporting Fig. S8B). The IHC revealed that RBM4-overexpressing tumors exhibited higher MVD (indicated by CD31-positive cells) than control tumors. The IHC staining (Ki-67) confirmed that both these effects can be rescued by interfering HNRNP-M and tumor proliferation(Fig. 8D). To explore the role of RBM4 in the hepatocellular carcinoma treatment, sorafenib (20 mg/kg) was administered to different groups of nude mice by intragastric administration. After four weeks , RBM4-knockout stopped the proliferation rate of hepatocellular carcinoma cells *in vivo* increasing the therapeutic effect of sorafenib significantly (Supporting Fig. S8B,C). Concludingly, RBM4 can promote angiogenesis *in vivo*, by directly binding RelA mRNA in the nucleus, and recruiting HNRNP-M to manage its stability via the WDR15 domain. Subsequently, the NF-kB signaling pathway is activated promoting the expression and secretion of VEGF-A, promoting the angiogenesis (Fig. 8E).

Discussion

Early metastatic HCC is a life-threatening disease for which no effective clinical treatment exists. Angiogenesis, a well-recognized characteristic of various cancers, including HCC, supplies nutrients to tumors besides facilitating the early metastasis of tumor cells by neovascularization [18]. Although previous studies have confirmed the effectiveness of anti-angiogenesis treatment for some tumor types, this therapeutic approach has various drawbacks [19]. Hence, elucidation of the molecular mechanisms

of disease progression with regard to angiogenesis is required to find new potential treatment targets [20].

NF-kB is a cardinal transcription factor in tumorigenesis, controling various downstream genes, including a few that promote angiogenesis, such as IL-6, IL-8, and VEGF-A. Unusual activation of the NF-kB signaling pathway has been confirmed in various cancers, including HCC [21]. During the development and progression of these diseases [22], several gene mutations aberrantly activate the NF-kB signaling pathway [23]. IkBa-mediated cytoplasmic accumulation of the heterodimer complex [24] is a key mechanism for terminating the NF-kB signaling [25]. However, ubiquitination- and phosphorylation-mediated signaling transduction regulates the activation of NF-kB [26]. For instance, Shouyu Wang *et al.* reported that ChIP interacted with NF-kB/p65 in gastric cancer, increasing its ubiquitination and degradation via the proteasome, terminating the NF-kB activity and inhibiting the IL-8-induced angiogenesis [27]. Yanfeng Liu *et al*. found that PROX1 increased the nuclear accumulation of p65 and stabilized p65 by recruiting ubiquitin-specific protease 7 (USP7), avoiding p65 degradation and enhancing the NF-kB signaling activity [28]. However, existance of new regulatory mechanisms in tumor cells is still unclear. We found that RBM4 stabilized RelA/p65 mRNA by recruiting HNRNP-M to enhance NF-kB signaling activity and specifically upregulate VEGF-A expression, providing a deeper understanding of this signaling pathway.

RBM4, also known as Lark, was initially known to play a role in the circadian rhythm regulation in *Drosophila* [29]. From an evolutionary perspective, RBM4 is highly conserved [30]. Through functional genomic screening and molecular approaches, we demonstrated that RBM4 has a key role in promoting HCC angiogenesis. As an RNA-binding protein, it functions by binding pre-mRNA to mediate alternative splicing [31]. For example, the RBM4-mediated upregulation of IR-B and MCL-1S inhibited the apoptotic resistance of breast cancer cells [32]. The RBM4 may have therapeutic potential with regard to excessive tau exon 10 inclusion as it plays a role in tau exon 10

alternative splicing[33], besides it's a role during growth and development. The energy metabolism of brown adipose tissue is also influenced by RBM4 through alternative splicing [34]. The RBM4 regulates Dab1 pre-mRNA splicing contributing to neuronal migration via Dab1 [35]. However, RBM4 has rarely been reported in cancer research. Lin *et al*. recently reported elevated levels of RBM4 in breast cancer cells and tissues, promoting the occurrence and development of breast cancer [32]. In contrast, Wang *et al*. revealed that RBM4 may exert a tumor suppressor role in lung cancer [36], and its overexpression inhibits the growth of cancer cells [37]. In another study, Markus *et al.* found that RBM4 knockdown decrease cell proliferation [38]. All these differing results are possible due to the complex genetic background and differences between tumors. In liver cancer tissues after surgical resection, decreased expression of RBM4 was observed as compared to the adjacent tissues, suggesting that decreased RBM4 levels correlate with poor prognosis in patients with hepatocellular carcinoma following hepatectomy [39]. Our results are contrary to this study. Herein, we found an increase in the expression of RBM4 in HCC tissues indicating poor prognosis in patients. These contradictory results illustrate the complexity of the underlying mechanism and hence, further investigations are warranted.

These findings revealed that high RBM4 expression is significantly correlated with cancer progression and may be used as an independent prognostic marker for overall survival rate in patients with HCC. The RBM4 promotes malignant phenotypes in cancer cells, specifically by accelerating angiogenesis through the NF-kB activation via HNRNP-M to synergistically stabilize RelA/p65 mRNA, hence selectively upregulating proangiogenic VEGF-A. These *in vitro* findings were confirmed in *in vivo* mouse models. Hence, we propose RBM4 as a potential novel prognostic marker for HCC and a therapeutic target for angiogenesis.

Acknowledgements

We sincerely thank the central Laboratory of Taizhou People's Hospital Affiliated to Nanjing Medical University and the school of Pharmacy of Nantong University for the help of instruments and equipment.

Fundings

This work was supported by the National Natural Science Foundation of China (81572397) and Scientific research start-up fund of The Affiliated Taizhou People's Hospital of Nanjing Medical University (QDJJ202106).

Author Contributions

Guoxiong Zhou and Jun Ye were responsible for the design and supervision of the experiment, Hexu Han completed the main part of the experiment in this study, Ting Lin and Zhenyu Wang assisted the development of experimental work, Jingjing Song was responsible for the bioinformatics analysis of this paper, and others have done a lot of supporting work in the implementation of this article.

Declaration of Interests Statement: The authors declare no potential conflicts of interest.

Availability of Data and Materials

All data generated or analyzed during this study are included in this published article.

Statement of Informed Consent

Written informed consent was obtained from a legally authorized representative(s) for anonymized patient information to be published in this article.

Ethics approval

All procedures performed in studies involving human participants were according to the standards upheld by the Ethics Committee of Affiliated Hospital of Nantong University and with those of the 1964 Helsinki Declaration and its later amendments for ethical research involving human subjects.

All animal experiments were approved by the Ethics Committee of Institutional Animal Care and Use Committee of Nantong University for the use of animals and conducted in accordance with the National Institutes of Health Laboratory Animal Care and Use Guidelines.

The animal experiment complies with the ARRIVE guidelines and in accordance with the National Institutes of Health guide for the care and use of Laboratory animals (NIH Publications No. 8023, revised 1978).

References

1. Craig A, von Felden J, Garcia-Lezana T, Sarcognato S, Villanueva AJNrG. Tumour evolution in hepatocellular carcinoma. Hepatology**,** 2020; 17: 139-52.
2. Hanahan D, Weinberg RA. Hallmarks of cancer: the next generation. Cell. 2011; 144: 646-74.
3. Raica M, Cimpean AM, Ribatti D. Angiogenesis in pre-malignant conditions. Eur J Cancer. 2009; 45: 1924-34.
4. Weidner N. Tumor angiogenesis: review of current applications in tumor prognostication. Semin Diagn Pathol. 1993; 10: 302-13.
5. Sugimachi K, Tanaka S, Terashi T, Taguchi K, Rikimaru T, Sugimachi K. The mechanisms of angiogenesis in hepatocellular carcinoma: angiogenic switch during tumor progression. Surgery. 2002; 131: S135-41.
6. Zhu A, Duda D, Sahani D, Jain RJNrCo. HCC and angiogenesis: possible targets and future directions. 2011; 8: 292-301.
7. Aggarwal B, Sung BJCd. NF-κB in cancer: a matter of life and death. 2011; 1: 469-71.
8. DiDonato JA, Mercurio F, Karin M. NF-κB and the link between inflammation and cancer. Immunol Rev. 2012; 246: 379-400.
9. Morgan D, Garg M, Tergaonkar V, Tan S, Sethi GJBebaRoc. Pharmacological significance of the non-canonical NF-κB pathway in tumorigenesis. 2020; 1874: 188449.
10. Lawrence T. The nuclear factor NF-kappaB pathway in inflammation. Cold Spring Harb Perspect Biol. 2009; 1: a001651.
11. Oeckinghaus A, Ghosh S. The NF-kappaB family of transcription factors and its regulation. Cold Spring Harbor perspectives in biology. 2009; 1: a000034.
12. Chen J, Chen ZJ. Regulation of NF-κB by ubiquitination. Current opinion in immunology. 2013; 25: 4-12.
13. Peretti D, Bastide A, Radford H, Verity N, Molloy C, Martin MG, et al. RBM3 mediates structural plasticity and protective effects of cooling in neurodegeneration. Nature. 2015; 518: 236-9.
14. Bechara E, Sebestyén E, Bernardis I, Eyras E, Valcárcel JJMc. RBM5, 6, and 10 differentially regulate NUMB alternative splicing to control cancer cell proliferation. 2013; 52: 720-33.

15. Jiang X, Liu B, Nie Z, Duan L, Xiong Q, Jin Z, et al. The role of m6A modification in the biological functions and diseases. 2021; 6: 74.
16. Chang H, Lin JJBebaMcr. SRSF1 and RBM4 differentially modulate the oncogenic effect of HIF-1α in lung cancer cells through alternative splicing mechanism. 2019; 1866: 118550.
17. Shrivastava A, Calame KJNar. An analysis of genes regulated by the multi-functional transcriptional regulator Yin Yang-1. 1994; 22: 5151-5.
18. Hanahan D, Weinberg RA. The hallmarks of cancer. Cell. 2000; 100: 57-70.
19. Jayson GC, Kerbel R, Ellis LM, Harris AL. Antiangiogenic therapy in oncology: current status and future directions. Lancet. 2016; 388: 518-29.
20. Moreno Garcia V, Basu B, Molife LR, Kaye SB. Combining antiangiogenics to overcome resistance: rationale and clinical experience. Clin Cancer Res. 2012; 18: 3750-61.
21. He G, Karin M. NF-κB and STAT3 - key players in liver inflammation and cancer. Cell Res. 2011; 21: 159-68.
22. Gadjeva M, Tomczak MF, Zhang M, Wang YY, Dull K, Rogers AB, et al. A role for NF-kappa B subunits p50 and p65 in the inhibition of lipopolysaccharide-induced shock. J Immunol. 2004; 173: 5786-93.
23. Kasibhatla S, Genestier L, Green DR. Regulation of fas-ligand expression during activation-induced cell death in T lymphocytes via nuclear factor kappaB. J Biol Chem. 1999; 274: 987-92.
24. Arenzana-Seisdedos F, Thompson J, Rodriguez MS, Bachelerie F, Thomas D, Hay RT. Inducible nuclear expression of newly synthesized I kappa B alpha negatively regulates DNA-binding and transcriptional activities of NF-kappa B. Mol Cell Biol. 1995; 15: 2689-96.
25. Arenzana-Seisdedos F, Turpin P, Rodriguez M, Thomas D, Hay RT, Virelizier JL, et al. Nuclear localization of I kappa B alpha promotes active transport of NF-kappa B from the nucleus to the cytoplasm. J Cell Sci. 1997; 110 (Pt 3): 369-78.
26. Liu S, Chen ZJ. Expanding role of ubiquitination in NF-κB signaling. Cell Res. 2011; 21: 6-21.
27. Wang S, Wu X, Zhang J, Chen Y, Xu J, Xia X, et al. CHIP functions as a novel suppressor of tumour angiogenesis with prognostic significance in human gastric cancer. Gut. 2013; 62: 496-508.
28. Liu Y, Zhang Y, Wang S, Dong QZ, Shen Z, Wang W, et al. Prospero-related homeobox 1 drives angiogenesis of hepatocellular carcinoma through selectively activating interleukin-8 expression. Hepatology. 2017; 66: 1894-909.
29. McNeil GP, Schroeder AJ, Roberts MA, Jackson FR. Genetic analysis of functional domains within the Drosophila LARK RNA-binding protein. Genetics. 2001; 159: 229-40.
30. Markus MA, Morris BJ. Lark is the splicing factor RBM4 and exhibits unique subnuclear localization properties. DNA Cell Biol. 2006; 25: 457-64.

31. Markus MA, Morris BJ. RBM4: a multifunctional RNA-binding protein. Int J Biochem Cell Biol. 2009; 41: 740-3.
32. Lin JC, Lin CY, Tarn WY, Li FY. Elevated SRPK1 lessens apoptosis in breast cancer cells through RBM4-regulated splicing events. RNA. 2014; 20: 1621-31.
33. Kar A, Havlioglu N, Tarn WY, Wu JY. RBM4 interacts with an intronic element and stimulates tau exon 10 inclusion. J Biol Chem. 2006; 281: 24479-88.
34. Chi YL, Lin JC. RBM4a modulates the impact of PRDM16 on development of brown adipocytes through an alternative splicing mechanism. Biochim Biophys Acta Mol Cell Res. 2018; 1865: 1515-25.
35. D D, Hung KY, Tarn WY. RBM4 Modulates Radial Migration via Alternative Splicing of Dab1 during Cortex Development. Mol Cell Biol. 2018; 38.
36. Qi Y, Yu J, Han W, Fan X, Qian H, Wei H, et al. A splicing isoform of TEAD4 attenuates the Hippo-YAP signalling to inhibit tumour proliferation. Nat Commun. 2016; 7: ncomms11840.
37. RBM4-regulated alternative splicing suppresses tumorigenesis. Cancer Discov. 2014; 4: 1253.
38. Markus MA, Yang YH, Morris BJ. Transcriptome-wide targets of alternative splicing by RBM4 and possible role in cancer. Genomics. 2016; 107: 138-44.
39. Chen JY, Liu LP, Xu JF. Decrease of RBM4 indicates poor prognosis in patients with hepatocellular carcinoma after hepatectomy. OncoTargets and therapy. 2017; 10: 339-45.

Figure legends

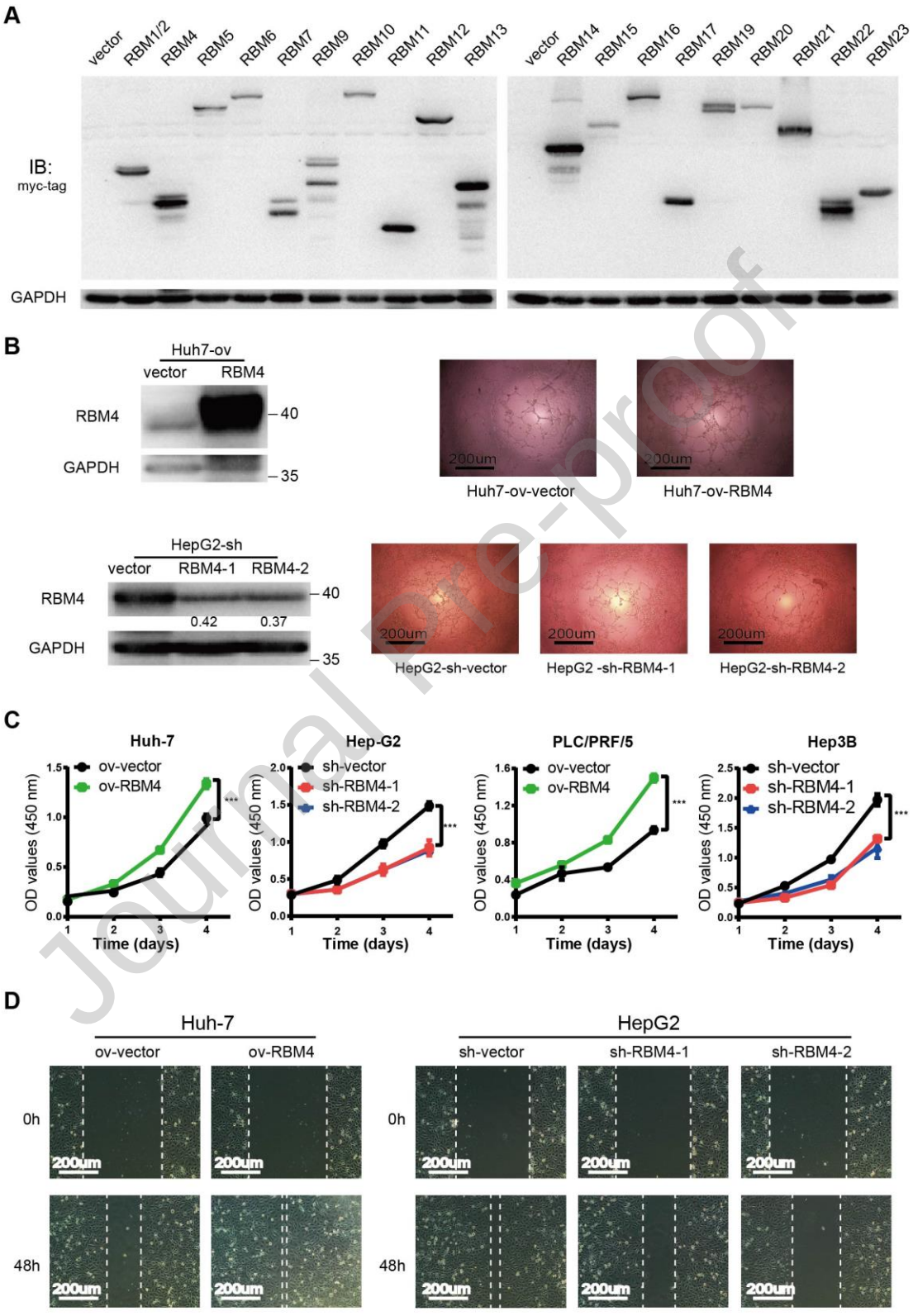

Figure 1. Role of RBM4 in promoting tumor angiogenesis

(A) The effect of overexpression of several RNA-binding proteins (RBPs) on angiogenesis in HCC cells. In the supplementary material (Figure S1A), tube formation assays show that the supernatant from Huh-7-ov-RBM4 cells significantly promoted the formation of complete tubular structures, while the supernatant from Huh7 cells overexpressing other RBPs had marginal or no effects.

(B) RBM4 protein levels analyzed by immunoblotting after establishing stable cell line.

(C) CCK8 assays revealing the supernatant from Huh-7/PLC/PRF/5-ov-RBM4 cells promoted HUVEC growth, whereas the stimulating effect of the supernatant from HepG2/Hep3B-sh-RBM4 cells on HUVEC growth was inconspicuous, Data represented as the mean ± S.D (**P < 0.01, ***P < 0.001).

(D) Wound healing assays demonstrating that supernatant from Huh-7-ov-RBM4 cells strongly promots the migration of HUVECs *in vitro*. The opposite effect can be observed in HepG2 cells when RBM4 was knocked down, Corresponding statistics shown in supplementary materials (Figure S1E).

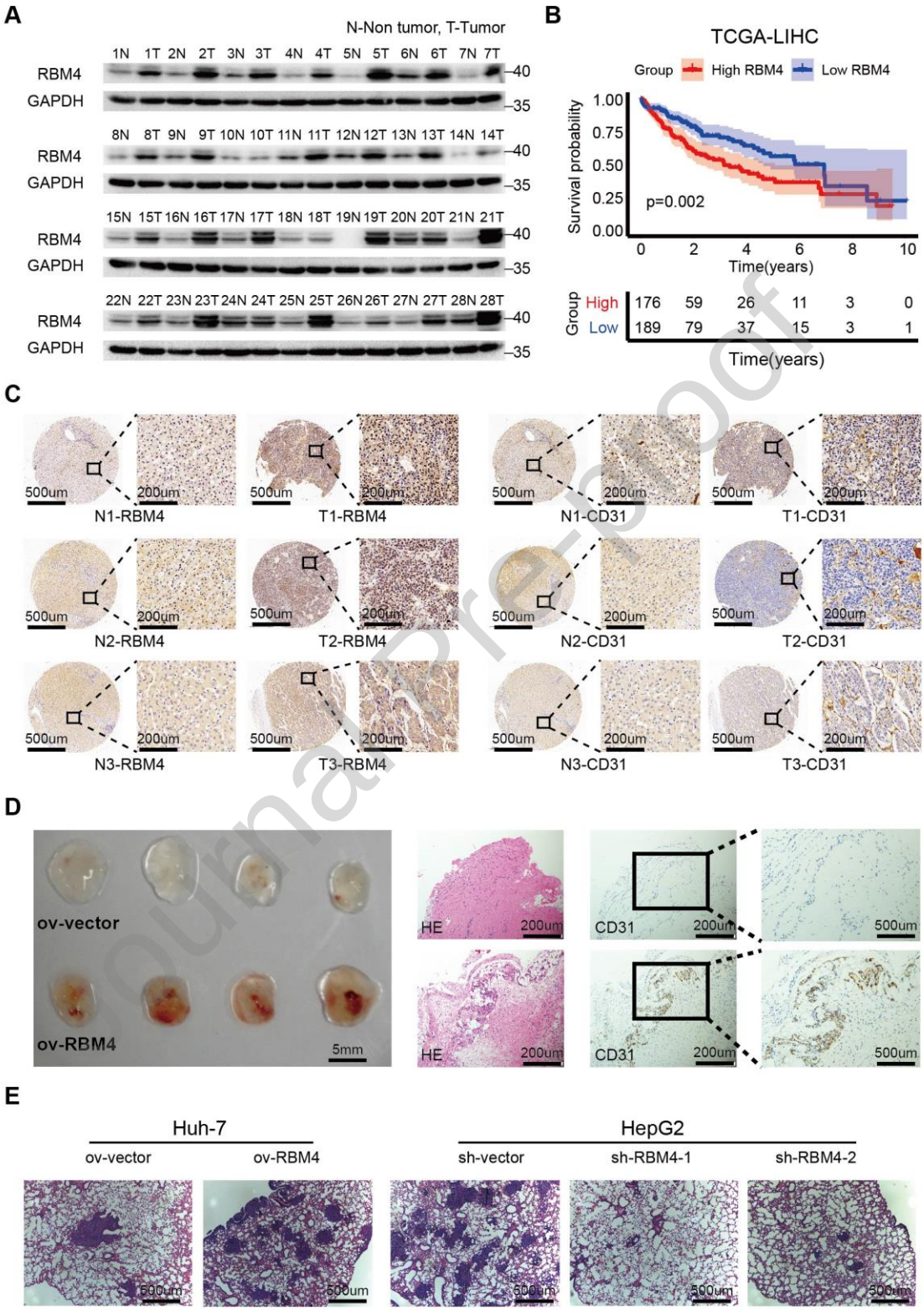

Figure 2. correlation between RBM4 upregulation and higher invasiveness and poor prognosis

(A) Western blot of RBM4 expression in 28 paired human HCC tumor tissues (T) and matching paracancerous tissues (N), showing that RBM4 is generally highly expressed in tumor tissues compared to adjacent tissues. Corresponding statistics are available in supplementary materials (Figure S2A).

(B) Kaplan–Meier analysis of overall survival (OS) of HCC patients with low versus high expression of RBM4 based on data from The Cancer Genome Atlas (TCGA), suggesting that increased RBM4 is correlated with poor prognosis ($P < 0.05$, log-rank test).

(C) IHC staining results of RBM4 and CD31 revealing that the expression of RBM4 and CD31 are increased in cancer tissue as compared to the corresponding adjacent tissues.

(D) Images of retrieved Matrigel plugs, indicating that compared with the control group, the matrigel from the supernatant of the overexpression RBM4 group has more vascular infiltration. The Matrigel plugs were fixed by paraformaldehyde (PFA), sectioned, and subjected to hematoxylin and eosin (H&E) and IHC staining (n = 4/group).

(E) Images showing representative H&E staining of lung tissue samples from the different experimental groups (n = 5/group).

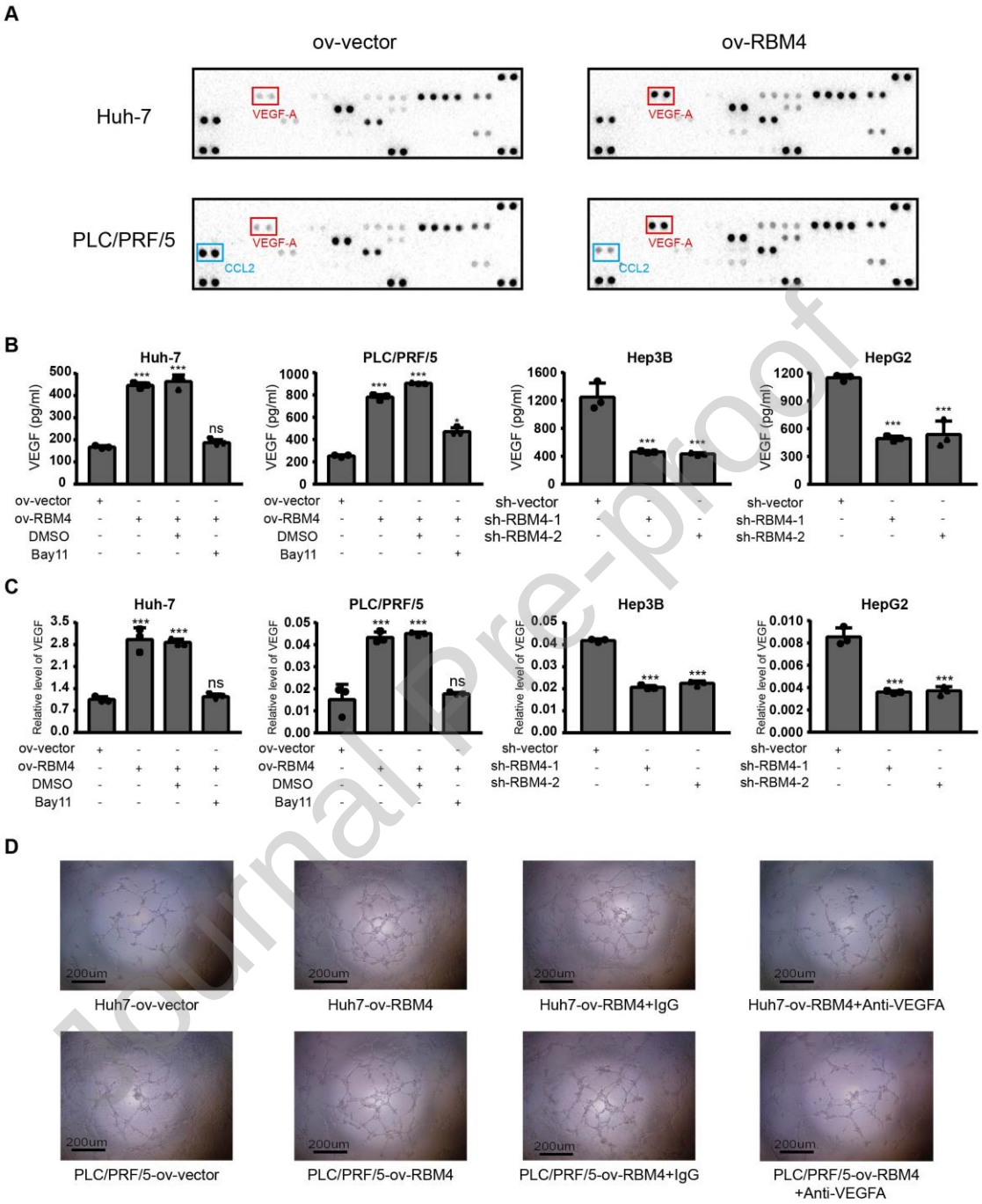

Figure 3. Relationship between RBM4 and angiogenesis shown by VEGF-A

(A) Screening of angiogenesis-related factors by proteomic antibody array in media collected from Huh-7-ov-RBM4 and PLC/PRF/5- ov-RBM4 cells and corresponding control cells, showing that after overexpression of RBM4, only the expression of VEGF-A was significantly increased.

(B) VEGF-A protein levels in supernatant from different cells as determined using ELISA. Data represented as the mean ± S.D (*P < 0.05, ***P < 0.001; ns, not significant).

(C) VEGF-A mRNA levels from different cells as determined using qRT-PCR analysis. Data represented as the mean ± S.D (*P < 0.05, **P < 0.01, ***P < 0.001; ns, not significant).

(D) Abrogation of the increased complete tubular structures formed by by VEGF-A antibody (500 ng/ml) addition to the conditioned medium.

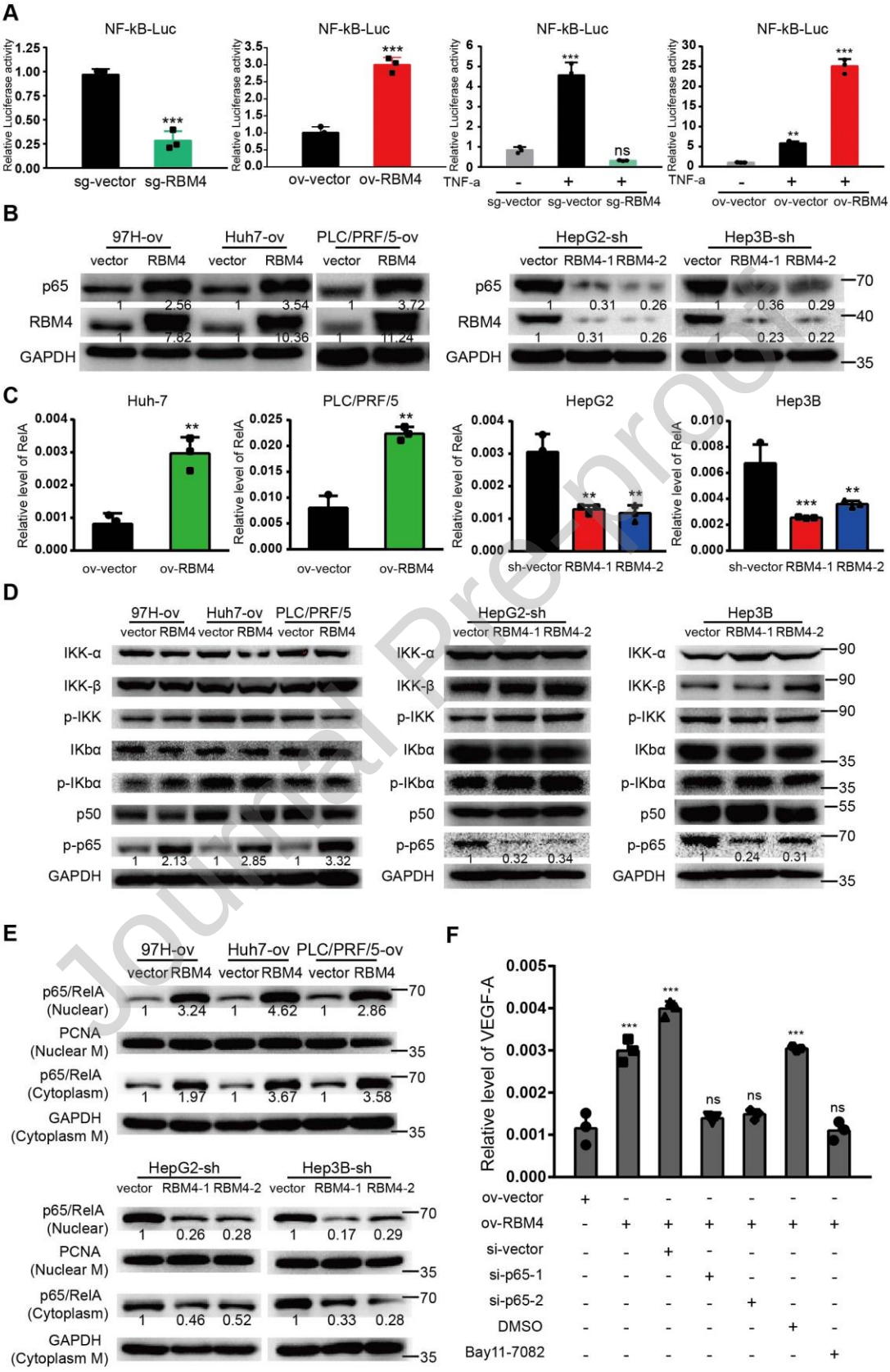

Figure 4. Role of RBM4 in promoting NF-kB activity and the expression of its target pro-angiogenesis genes

(A) Dual-luciferase reporter assay showing that RBM4 overexpression in HEK-293T cells enhanced NF-kB activity, whereas RBM4 knockout in HEK-293T cells inhibited NF-kB activity. Similar results were verified externally, when treating with tumor necrosis factor-a (TNF-a) (10ng/ml). Dual-luciferase reporter assay showing that RBM4 overexpression enhanced NF-kB activity, whereas RBM4 knockout inhibited NF-kB activity. Dual-luciferase reporter assay showing that RBM4 overexpression enhanced NF-kB activity, whereas RBM4 knockout inhibited NF-kB activity. Data represented as the mean ± S.D (*P < 0.05, **P < 0.01, ***P < 0.001; ns, not significant).

(B) Determination of protein levels in indicated cells by immunoblotting.

(C) qRT-PCR showing influence of RBM4 expression on RelA/p65 mRNA levels.. Data represented as the mean ± S.D (**P < 0.01, ***P < 0.001).

(D) Immunoblotting showing that protein levels of other molecules in the canonical NF-kB signaling pathway are not affected by RBM4 overexpression/knockout.

(E) Western blot of nuclear p65 and cytoplasmic p65 in different cells. PCNA was used as a nuclear loading control, whereas GAPDH was used as a cytoplasmic loading control.

(F) The qRT-PCR results for VEGF mRNA levels. Results shown as the mean ± S.D (*P < 0.05, **P < 0.01, ***P < 0.001)

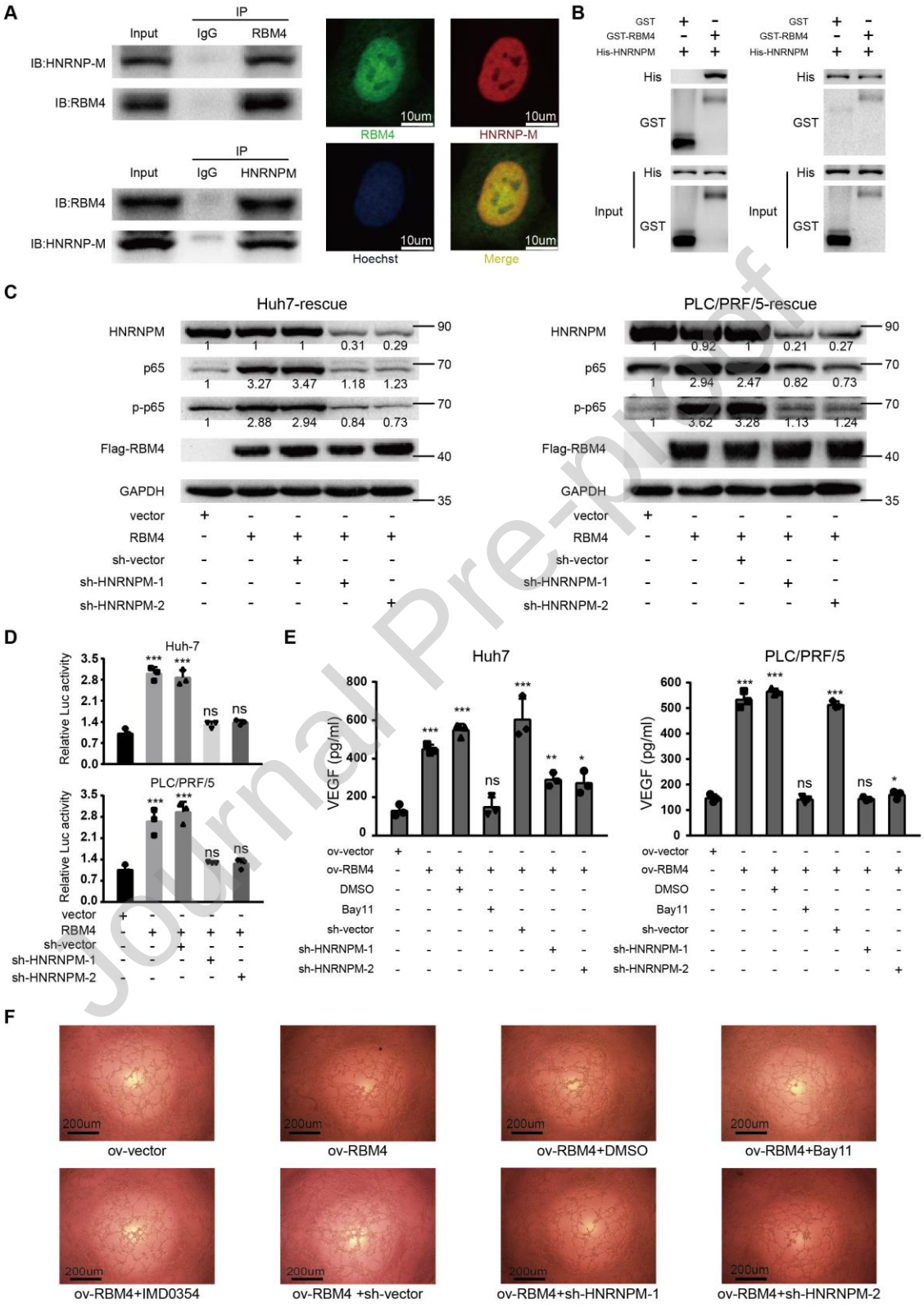

Figure 5. RBM4 recruits HNRNP-M to active NF-kB pathway

(A) Immunoprecipitation (IP) showing protein–protein interaction between RBM4 and HNRNP-M in HEK293T cells with the corresponding antibodies followed by immunoblotting. IgG was used as a negative control (left). Endogenous RBM4 co-localized with HNENP-M in the nucleus as revealed using immunofluorescence (right).

(B) Protein purification and pulldown results confirming the direct interaction between RBM4 and HNRNP-M.

(C) Western blot demonstrating that the upregulation of RelA/p65 caused by changes in RBM4 expression could be rescued by knocking down HNRNP-M in Huh-7 and PLC/PRF-5 cells.

(D) Dual-luciferase reporter assay showing that knocking down HNRNP-M in Huh-7/PLC/PRF/5-ov-RBM4 cells can rescue the increased activity of NF-kB activity caused by the RBM4-overexpression. Data shown as the mean ± S.D (*P < 0.05, **P < 0.01, ***P < 0.001; ns, not significant).

(E) Enzyme-linked immunosorbent assay (ELISA) showing that blocking NF-kB signaling or interfering with HNRNP-M could rescue the increased secretion of VEGF-A caused by RBM4 overexpression in Huh-7 and PLC/PRF-5 cells. Data represented as the mean ± S.D (*P < 0.05, **P < 0.01, ***P < 0.001; ns, not significant).

(F) Tube formation assays showing that blocking NF-kB signaling or interfering with HNRNP-M could rescue the increased number of complete tubular structures following treatment with supernatant from Huh-7-ov-RBM4 cells. Corresponding statistics are shown in supplementary materials (Figure S5J).

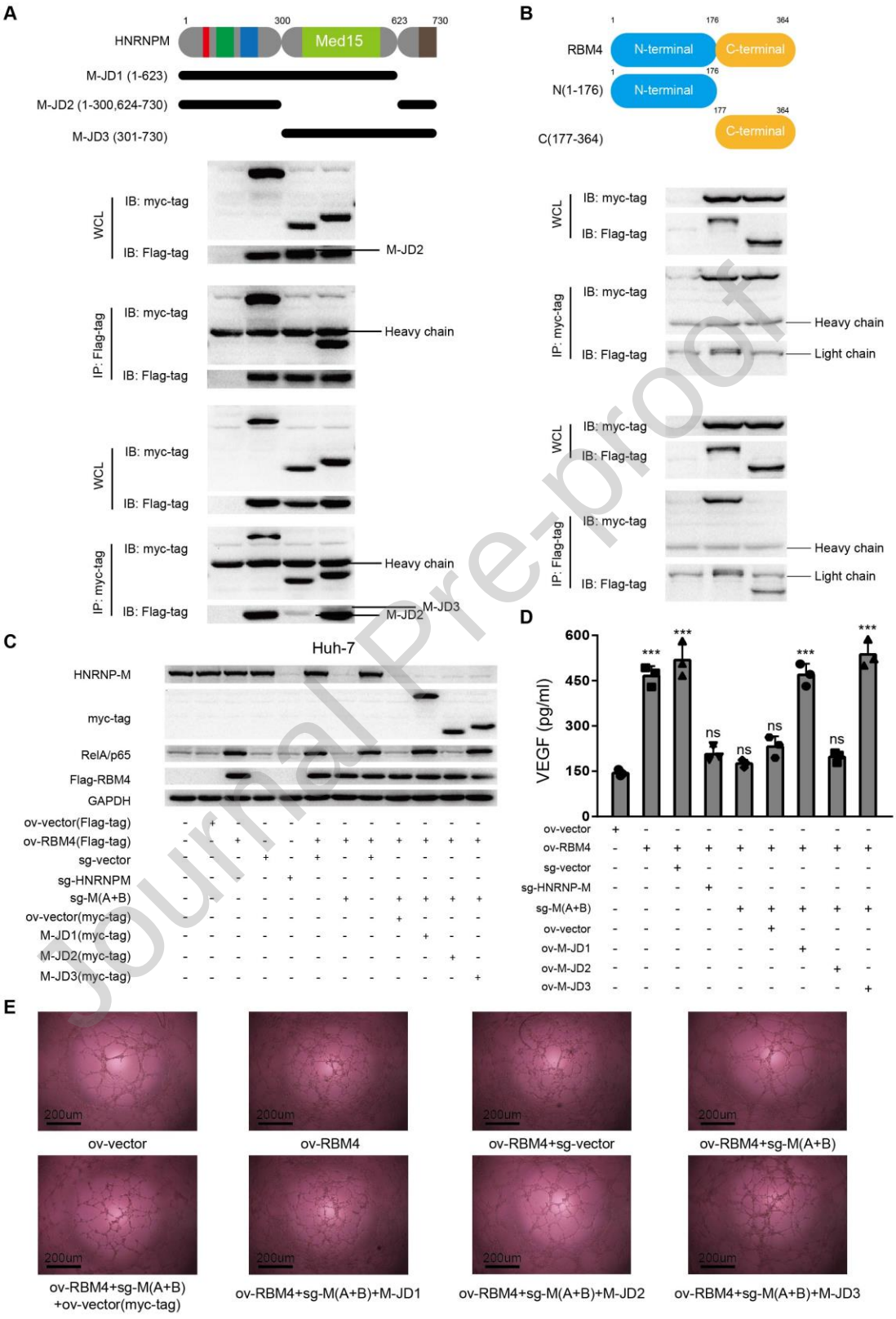

Figure 6. Correlation between WDR15 domain of HNRNP-M and the function of the RBM4–HNRNP-M interaction

(A) Co-IP of HEK293T cells transfection with the indicated FLAG-tagged-RBM4 and Myc-tagged-HNRNP-M truncations showing the interaction between HNRNPM and RBM4 depends on the WDR15 domain of HNRNPM. Schematic diagrams of HNRNP-M. Its truncated mutants are also shown (upper).

(B) Co-IP of HEK293T cells transfection with the indicated Myc-tagged-HNRNP-M and FLAG-tagged-RBM4 truncations showing the interaction between RBM4 and HNRNPM depends on the N-terminal domain of RBM4. Schematic diagrams of RBM4. Its truncated mutants are also shown (upper).

(C) Western blot revealing role of the WDR15 domain of HNRNP-M in activation of NF-kB signaling by the overexpression of RBM4 in Huh-7 cells.

(D) Enzyme-linked immunosorbent assay (ELISA) suggesting that deleting the WDR15 domain of HNRNP-M could rescue the increased secretion of VEGF-A caused by RBM4 overexpression. Data represent the mean ± S.D (*P < 0.05, ***P < 0.001; ns, not significant).

(E)Tube formation assays demonstrating that deleting the WDR15 domain of HNRNP-M could rescue the increased number of complete tubular structures following treatment with supernatant from Huh-7-ov-RBM4 cells. Corresponding statistics shown in supplementary materials (Figure S6F).

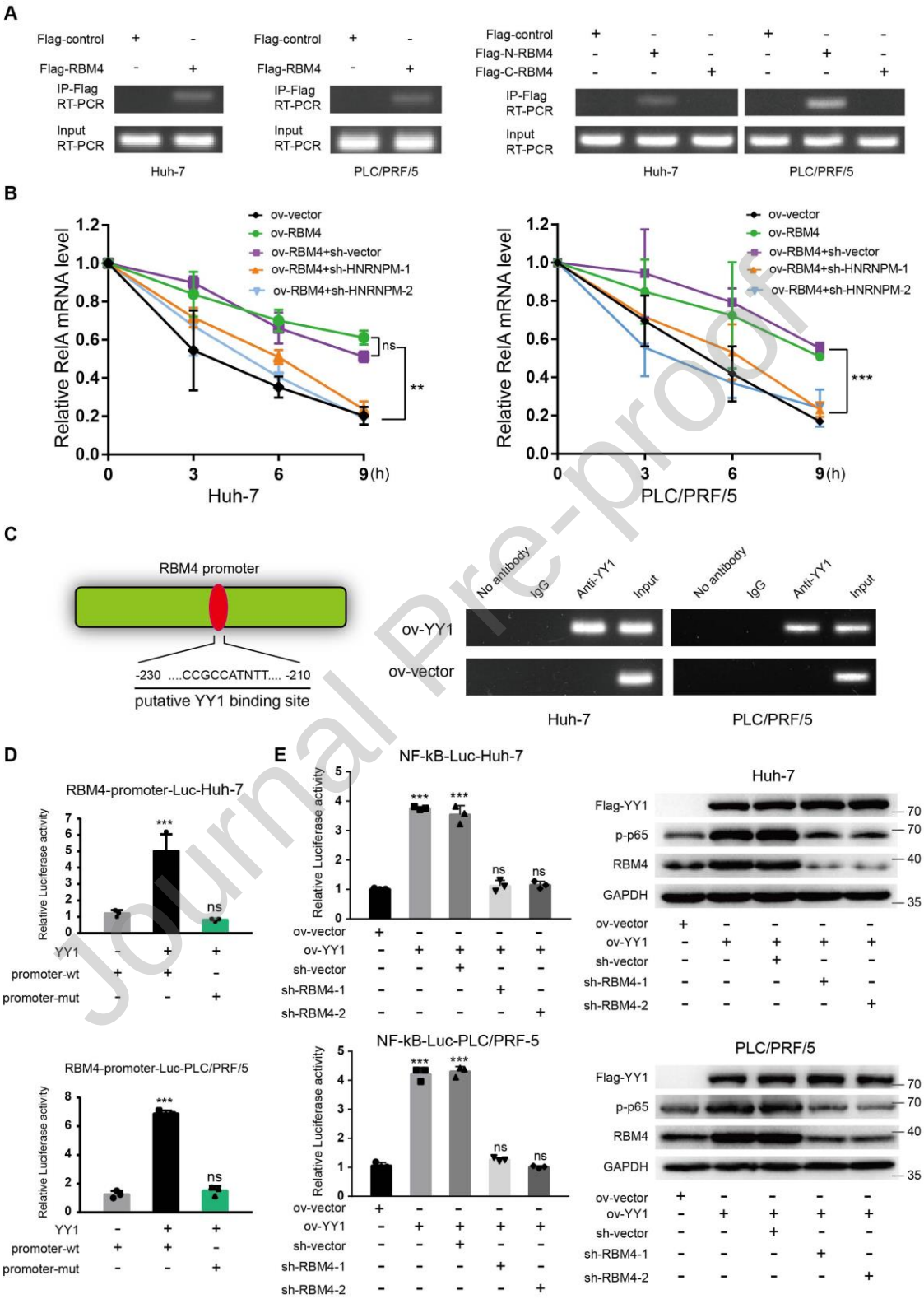

Figure 7. Correlation between N-terminal of RBM4 and p65 stability

(A) Direct binding of RelA/p65 mRNA with RBM4 examined through RNA immunoprecipitation (RIP) assays in Huh-7 and PLC/PRF-5 cells exogenously expressing FLAG-tagged-RBM4 or a control vector (left). Direct binding of RelA/p65 mRNA with N-terminal of RBM4 examined by RNA immunoprecipitation (RIP) assays in Huh-7 and PLC/PRF-5 cells exogenously expressing FLAG-tagged-RBM4 truncations or a control vector (right).

(B) Analysis of the stability of RelA/p65 mRNA in different groups of Huh-7/PLC/PRF/5 cells after actinomycin D treatment (10 μg/ml in fresh medium). Time points of harvested cells showing the overexpression of RBM4 improved the stability of RelA/ P65 mRNA, while the effect was recovered after knocking down HNRNPM. Data represented as the mean ± S.D (**P < 0.01, ***P < 0.001; ns, not significant).

(C) Schematic diagram of possible binding sites of YY1 in the RBM4 promoter region (left). ChIP assay confirming the interaction between YY1 and the promoter of RBM4 (right).

(D) Dual-luciferase reporter assays suggesting that YY1 could really initiate the transcription of RBM4 in Huh-7 cells. Data represent the mean ± S.D (***P < 0.001; ns, not significant).

(E) Dual-luciferase reporter assays and Western blotting assays indicating the role of RBM4 in completely blocking the activation of NF-kB signaling by YY1 in Huh-7 and PLC/PRF/5 cells. Data represented the mean ± S.D (***P < 0.001; ns, not significant).

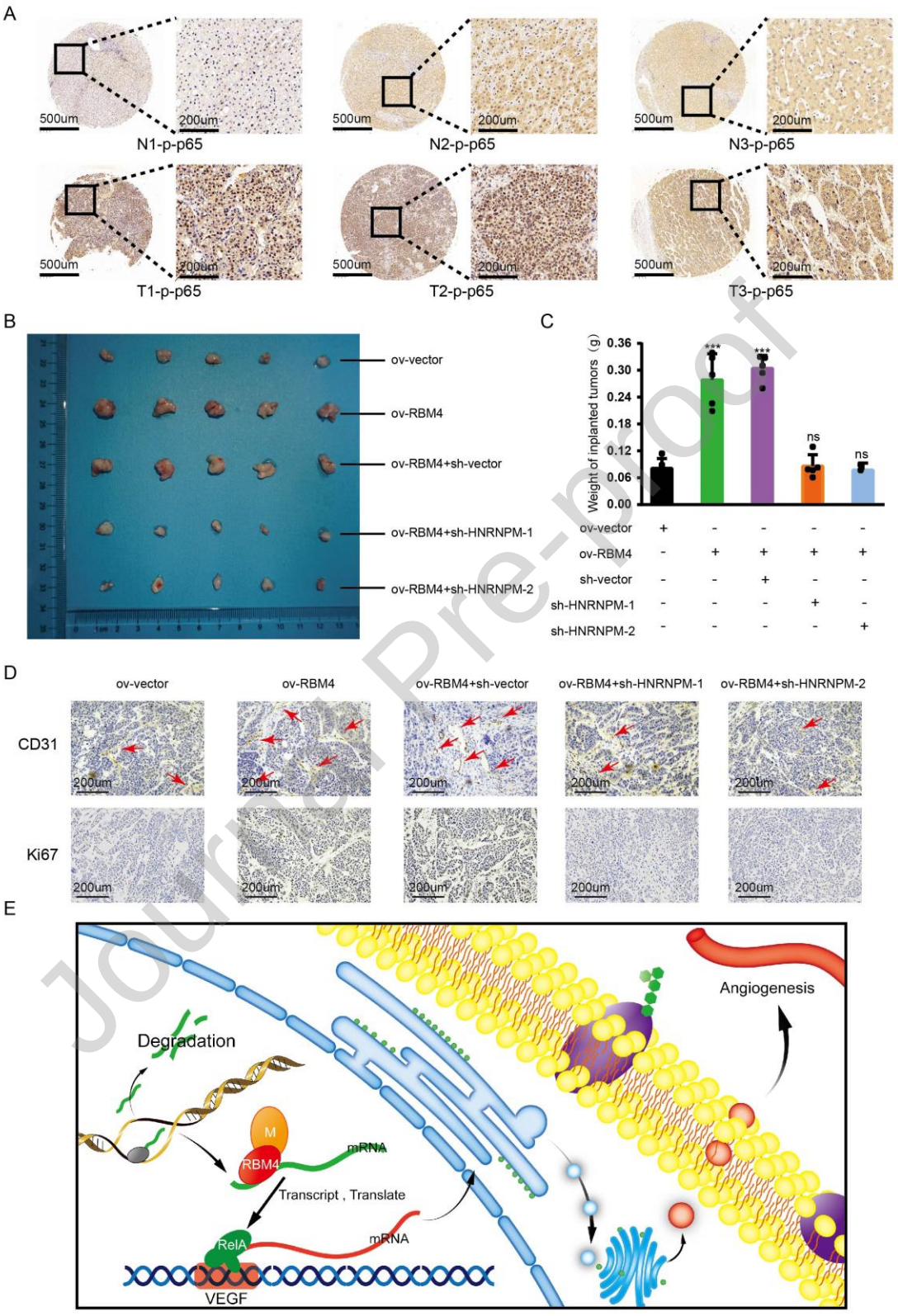

Figure 8. ***In vivo*** **RBM4 overexpression in cancer cells promotes angiogenesis**

(A) IHC staining indicating a higher expression of p-p65 in cancer samples versus corresponding normal tissues, the chip is from the same group as in Fig.2.

(B and C) Effect of RBM4 overexpression on the growth of tumor xenografts in nude mice, whereas knockdown of HNRNP-M repressed this effect. (B) The left panel showing photographs of the tumors. (C) The right panel showing the weight of tumors after 28 days. Data represented as the mean ± S.D (***P < 0.001; ns, not significant).

(D) IHC staining of tumor microvessel density (indicated by CD31-positive cells) and related proliferation indexes (Ki-67) in the different groups described above.

(E) A proposed model illustrating the function, expression, and biological mechanism of RBM4 in tumor angiogenesis.

Figure S1. Role of RBM4 in promoting tumor angiogenesis

(A) The tube formation assays results showing that the supernatant from Huh-7-ov-RBM4 cells significantly promoted the formation of complete tubular structures, while the supernatant from Huh7 cells overexpressing other RBPs had marginal or no effects. Data represented as the mean ± S.D (*P < 0.05, ***P < 0.001; ns, not significant).

(B) Western blot of RBM4 and YY1 expression in different HCC cell lines (left), qPCR assays of RBM4 mRNA levels in different HCC cell lines (right).

(C) RBM4 protein levels suggested by immunoblotting.

(D) Statistical analysis of the different groups of tube formation assays, Data represented as the mean ± S.D (***P < 0.001).

(E) Statistical analysis of the wound healing assays of human umbilical vein endothelial cells (HUVEC) stimulated by cell supernatants from different HCC cell groups in the text. Data represented as the mean ± S.D (**P < 0.01, ***P < 0.001).

Figure S2. Correlation between **RBM4 upregulation and increased invasiveness and poor prognosis**

(A) The RBM4 expression in cancer tissues is significantly higher than in adjacent tissues. Results expressed as mean ± S.D (***P < 0.001).

(B) (a) Analysis of RBM4 expression in the hepatocellular carcinoma group in the TCGA database and GSE76427 (***P < 0.001). (b) The Kaplan-Meier survival curves, showing correlation between increased expression of RBM4 with the poor DSS, DFS, and PFS in the TCGA database. DSS, disease-specific survival; DFS, disease-free survival; PFS, progression-free survival. (c) Different HCC cohort, GSE76427, showing correlation between higher RBM4 expression and a poor OS (p = 0.052). (d) Correlation between RBM4 mRNA levels and higher grade in cancerous tissues, as well as higher tumor stage. (e) Correlation between high RBM4 expression and poor OS (HR = 2.05, p = 0.003). (f) Multivariable Cox regression analyses suggesting the significant prognostic factors.

(C) A significant positive correlation between the o RBM4 levels and MVD (indicated by CD31-positive cells).

(D) Quantitative RT-PCR and immunoblotting analysis of endothelial cells gene markers CD31 and VE-cadherin (VE-cad) from different experiment groups in Huh-7 cells. Data represented as the mean ± S.D (**P < 0.01, ***P < 0.001).

(E) Images of Matrigel plugs retrieved from different experiment groups. Data represented as the mean ± S.D. (**P < 0.01, ***P < 0.001).

(F) The incidence of lung metastasis in the mouse lung tissues from tail vein metastasis mice model after 4 weeks of injection..

Figure S3. RBM4 promotes angiogenesis through VEGF-A

(A) RNA immunoprecipitation (RIP) assays showing that RBM4 did not directly bind to VEGF-A mRNA in Huh-7 and PLC/PRF/5 cells.

(B) Results of transcriptome sequencing.

Figure S4. Promotion of the NF-kB activity by RBM4 and the expression of its target pro-angiogenesis genes

(A) Changes in RBM4 does not affect the expression of HIF-1a, VHL, SP1, STAT3, TP53, Fos, and c-JUN. Culturing the cells of each group in a hypoxic environment with 1% oxygen for 16 h suggested the expression of HIF-1a. Data represented as the mean ± S.D. (ns, not significant).

(B) Dual-luciferase reporter assay showing the role of RBM4 overexpression and knockout in the NF-kappa B pathway activation. Data represented as the mean ± S.D. (**P < 0.01, ***P < 0.001; ns, not significant).

(C) Immunoblotting indicating protein levels in HEK-293T cells.

(D) Immunoblotting indicating effect of RBM4 alteration in HEK-293T cells on the protein levels of other molecules in the canonical NF-kB signaling pathway.

(E) Immunofluorescence showing effect of RBM4 overexpression on the expression of RelA/p65 in HEK-293T cells.

(F) Western blots of nuclear p65 and cytoplasmic p65 in HEK-293T cells. PCNA was used as the nuclear loading control and GAPDH was used as the cytoplasm loading control.

(G) Evaluation of the mRNA levels of VEGF-A in HEK-293T-ov-RBM4 and HEK-293T-sg-RBM4 cells by qRT-PCR. Data represented as the mean ± S.D (***P < 0.001).

Figure S5. RBM4 interacts with HNRNP-M to execute its function.

(A) Cellular extracts of FLAG-RBM4 separated by SDS-PAGE, and subjected to Coomassie brilliant blue staining to verify the immunoprecipitation (IP) results. The extracts were later analyzed by mass spectrometry.

(B) Screening of the candidate molecules obtained in mass spectrometry by using CRISPR-Cas9 technology suggesting HNRNP-M as the most likely interaction candidate.

(C) Effect of knocking out HNRNP-M in HEK-293T and Huh-7 cells on the quantity of RelA/p65 and p-p65, and the expression of VEGF-A. Data represented as the mean ± S.D (ns, not significant).

(D) To rule out to promote tube formation, we respectively knocked out DDX5 in Huh-7/PLC/PRF/5-ov-RBM4 cells. Tube formation assays showing the role of DDX5 in RBM4 increasing the activity of NF-kB signaling pathway. Data represented as the mean ± S.D (ns, not significant)..

(E) Endogenous protein–protein interaction between RBM4 and HNRNP-M in HepG2 and Hep3B cells, followed by immunoblotting. IgG is a negative control for immunoprecipitation.

(F) Co-IP analysis of HEK-293T cell lysates treated with RNase.

(G) The upregulation of RelA/p65 rescued by knocking out HNRNP-M in HEK-293T cells.

(H) The VEGF mRNA level confirming the effect of knocking down HNRNP-M on rescuing increased VEGF levels in Huh-7 and PLC/PRF/5 cells. Data represented as the mean ± S.D (***P < 0.001, ns, not significant).

(I) Tube formation assays showing the effect of blocking of NF-kB signaling or interfering with HNRNP-M on rescuing the increased number of complete tubular structures .

(J) Statistical analysis of the results of the different groups of tube formation assays. Data represented as the mean ± S.D (***P < 0.001, ns, not significant).

Figure S6. Role of the WDR15 domain of HNRNP-M for the function of the RBM4–HNRNP-M interaction.

(A) The pull-down results of Co-IP by analyzing the binding between RBM4 truncated mutant protein and HNRNP-M full-length protein, and the binding between HNRNP-M truncated mutant protein and RBM4 full-length protein.

(B) Different strategies of knocking out the HNRNP-M gene.

(C) Western blot revealing the role of WDR15 domain of HNRNP-M in NF-kB signaling activation by RBM4 overexpression in PLC/PRF/5 cells.

(K) (D) Enzyme-linked immunosorbent assay (ELISA) demonstrating that deletion of the WDR15 domain of HNRNP-M saves the increased secretion of VEGF-A caused by RBM4 overexpression. Results expressed as the mean ± S.D (***P < 0.001, ns, not significant).

(E) Tube formation assays indicating that deleting the WDR15 domain of HNRNP-M can save the increased number of complete tubular structures following treatment with supernatant from PLC/PRF/5-ov-RBM4 cells.

(F) Statistical analysis of the results of the different groups of tube formation assays. Data represented as the mean ± S.D (***P < 0.001).

Figure S7. Requirement of the N-terminal of RBM4 for p65 stability

(A) RNA immunoprecipitation (RIP) assays suggesting that HNRNP-M does not directly bind to RelA/p65 mRNA in Huh-7 and PLC/PRF/5 cells.

(B) RBM4 can directly bind to the RelA/p65 mRNA through its N-terminal in HEK-293T cells suggested by RNA immunoprecipitation (RIP) assays .

(C) Evaluation of the RelA/p65 mRNA stability in HepG2 cells after actinomycin D treatment (10 μg/ml added to the fresh medium) by qRT-PCR. Data representing the mean ± S.D (*P < 0.05, **P < 0.01).

(D) Evaluation of the RelA/p65 mRNA stability in HEK-293T cells after actinomycin D treatment (10 μg/ml added to the fresh medium) by qRT-PCR. Results expressed as the mean ± S.D (*P < 0.05, **P < 0.01, ns, not significant).

(E) Overexpression of different proteins in HEK-293T cells to screen the candidates influencing the expression of RBM4, and YY1.

(F) Overexpression and knocking out YY1 in Huh-7 and HepG2 cells suggesting that YY1 can affect the expression of RBM4.

(G) Immunoblotting and qRT-PCR showing the protein and mRNA levels of RBM4in YY1-overexpressed and respective control vector (ctrl)-transfected HEK-293T cells (upper). The protein and mRNA levels of RBM4 in YY1 knockdown (shRNA) and their respective control vector (ctrl)-transfected HEK-293T cells (down).

(L) Dual-luciferase reporter and Western blot indicating tentative role of RBM4 in blocking the NF-kB signaling activation by YY1 in HEK-293T cells. Results expressed as the mean ± S.D (***P < 0.001).

Figure S8. *In vivo* RBM4 overexpression in cancer cells

(A) A significant positive correlation between the RBM4 levels and the activation of NF-kB signaling pathway (indicated by p-p65-positive cells).

(B) Mice euthanized at the end of the experiment.

(C) The RBM4 knockout in HepG2 cells significantly reduced the proliferation rate in nude mice as compared to the corresponding control cells. Addition of sorafenib increased the drug sensitivity in cells in the HepG2-sg-RBM4 group compared to the control group (left), The statistical chart on the right reflecting the different tumor weights (right). Data expressed as the mean ± S.D (***P < 0.001).

Graphical abstract

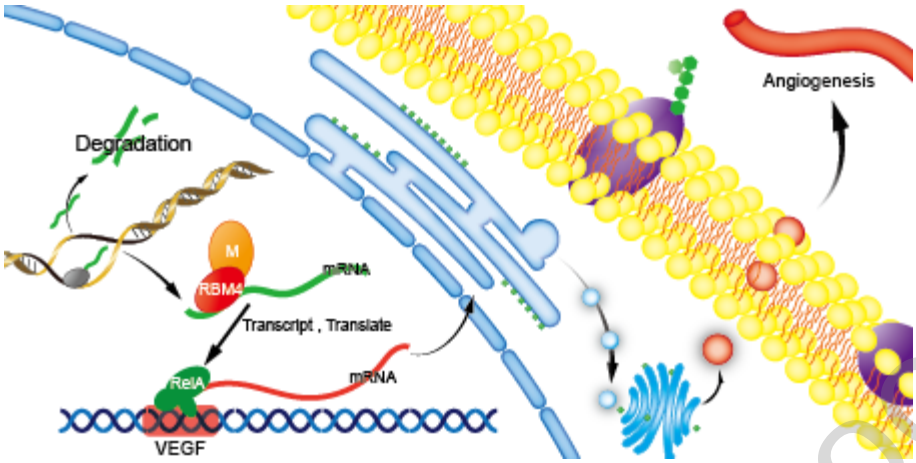

Author Contributions

Guoxiong Zhou and Jun Ye were responsible for the design and supervision of the experiment, Hexu Han completed the main part of the experiment in this study, Ting Lin and Zhenyu Wang assisted the development of experimental work, Jingjing Song was responsible for the bioinformatics analysis of this paper, and others have done a lot of supporting work in the implementation of this article.